DETERMINATION OF STRESS INTENSITY FACTORS IN A THICK-WALLED CYLINDER WITH MULTIPLE AXIAL CRACKS USING THE ENERGY BASED FINITE ELEMENT METHOD

KENNETH KARANJA KIRAGU

MASTER OF SCIENCE

(Mechanical Engineering)

JOMO KENYATTA UNIVERSITY OF AGRICULTURE AND TECHNOLOGY

2011

Determination of stress intensity factors in a thick-walled cylinder with multiple axial cracks using the energy based finite element method

Kenneth Karanja Kiragu

A thesis submitted in partial fulfilment for the degree of Master of Science in Mechanical Engineering in the Jomo Kenyatta University of Agriculture and Technology

2011

DECLARATION

This thesis is my original work and has not been presented for a degree in any other university.

Signature:..... Date:.....

Kenneth Karanja Kiragu

This thesis has been submitted for examination with our approval as the university supervisors.

Signature:..... Date:.....

Eng. Prof. J. M. Kihiu

JKUAT, Kenya

Signature:..... Date:.....

Dr. J. N. Keraita

Kimathi University College of Technology, Kenya

DEDICATION

This work is dedicated to my wife Esther and my son Chris.

ACKNOWLEDGEMENT

I would like to sincerely thank my supervisors Eng. Prof. J. M. Kihiu and Dr. J. N. Keraita for their advice and guidance throughout the research period. I am indebted to Mr. Bosco Byiringiro, Miss. Teresia Muthoni, Mr. Anthony Gitahi, Mr. Robert Kiplimo and Mr. Kamau Njuguna for their assistance in getting some of the very important papers needed in this research. I should not fail to mention the input of the chief technician Mr. Kibiro who made sure that computers were available together with the necessary softwares.

My special thanks also goes to my fellow students Peter Weramwanja, John Machira, Bernard Munyazikwiye, Jackson Githu, Grace Wairimu and Rehema Ndeda for their encouragement and assistance in various issues regarding this research. Finally, I would like to thank my parents, brothers, sisters, friends and my family for their prayers and encouragement throughout the research period.

TABLE OF CONTENTS

LIST OF TABLES

LIST OF FIGURES

APPENDIX

NOMENCLATURE

a	Crack length (m)
a_1	The major axis of an elliptical hole (m)
A_1, A_2	Lame's constants
b	Thickness of the flat plate (m)
b_1	The minor axis of an elliptical hole (m)
B_1 & B_2	Parameters of R_N
C_1 to C_6	Parameters of K_s
d	Inter-crack spacing (m).
E	Young's modulus of elasticity (N/m^2)
E*	Plane strain Young's modulus of elasticity (N/m^2)
$F_1(n)$	A parameter of K_{IP} which depends on the number of cracks
$F_2(a/d)$	A parameter of K_{IP} which depends on the inter-crack aspect ratio
$F_{x,i}$	Force transmitted in the x direction at location x_c (N)
$F_{y,i}$	Force transmitted in the y direction at location x_c (N)
g	Boundary number.
J-integral	A contour integral characterizing the strain energy release rate for a non-linear elastic material
Js	A parameter of K_{s2}
K	Stress intensity factor ($N/m^{1.5}$)

$\mathbf{K_{1N}}$	Stress intensity factor expressed as a function of N ancillary stress intensity factor ($N/m^{1.5}$)
$\mathbf{K_e}$	Stress intensity factor term corresponding to boundary-to-boundary interaction ($N/m^{1.5}$)
$\mathbf{K_f}$	Stress concentration factor
$\mathbf{K_h}$	Non-dimensional stress intensity factor obtained from literature
$\mathbf{K_g}$	Stress intensity factor for a body with g boundaries ($N/m^{1.5}$)
$\mathbf{K_I}$	Mode I stress intensity factor ($N/m^{1.5}$)
$\mathbf{K_{II}}$	Mode II stress intensity factor ($N/m^{1.5}$)
$\mathbf{K_{III}}$	Mode III stress intensity factor ($N/m^{1.5}$)
$\mathbf{K_{IA}}$	K for different configurations of crack arrays and various levels of autofrettage ($N/m^{1.5}$)
$\mathbf{K_{IP}}$	The K due to internal pressure for different crack arrays and for a wide range of crack lengths in non-autofrettaged cylinders ($N/m^{1.5}$)
$\mathbf{K`_I}$	Mode I stress intensity factor as a function of distance r ($N/m^{1.5}$)
$\mathbf{K`_{II}}$	Mode II stress intensity factor as a function of distance r ($N/m^{1.5}$)
$\mathbf{K_k}$	Non-dimensional stress intensity factor obtained from literature
$\mathbf{K_m}$	Non-dimensional stress intensity factor obtained using the modified virtual crack closure technique
$\mathbf{K_0}$	Stress intensity factor for a body without boundaries ($N/m^{1.5}$)
$\mathbf{K_s}$	Non-dimensional stress intensity factor obtained from literature
$\mathbf{K_{s2}}$	A parameter of K_z

$\mathbf{K_{sc}}$	Stress intensity factor obtained from literature for a cylinder with a single crack ($N/m^{1.5}$)
$\mathbf{K_{xc}}$	Stress intensity factor at x_c ($N/m^{1.5}$)
$\mathbf{K_z}$	Non-dimensional stress intensity factor obtained from literature
L	A parameter of R_s
$\mathbf{L_1}$	Crack length for the first subarray, i.e, fixed cracks (m)
$\mathbf{L_2}$	Crack length for the second subarray, i.e, varying cracks (m)
m	Distance between two consecutive nodes along the crack tip (m)
M	A function of cylinder geometry, crack length and number of cracks
n	Number of radial cracks in a cylinder
N	Number of boundaries in a cracked structure which is also equal to the number of ancillary configurations
$\mathbf{P_i}$	Internal pressure acting on the cylinder (N/m^2)
$\mathbf{P_o}$	External pressure acting on the cylinder (N/m^2)
r	A variable distance from the crack tip along the x axis where K can be calculated when $r \neq 0$ (m)
R	Radial distance of the crack tip from the centre of the cylinder (m)
$\mathbf{R_i}$	Inner radius of the cylinder (m)
$\mathbf{R_N}$	A parameter of K_h
$\mathbf{R_o}$	Outer radius of the cylinder (m)
$\mathbf{R_s}$	A parameter of K_Z

t	Thickness of the cylinder (m)
u	Displacement vector
$\mathbf{u_y}$	Crack tip displacement in y direction (m)
V	Traction vector
w	Strain energy density per unit volume (J/m^2)
$\mathbf{X_i}$	Nodal force at node i acting in radial direction (N)
$\mathbf{x_c}$	Distance from the crack tip to the intermediate location between the node under consideration and the next node (m)
Y	Ratio of the outer diameter to the inner diameter of the cylinder
$\mathbf{Z_i}$	Nodal force at node i acting in circumferential direction (N)
α	A parameter of K_{sc}
β	A parameter of R_N
μ	Poisson's ratio
κ	A parameter of u_x and u_y
λ	A dimensionless factor which depends on the geometry of the specimen or structural component
ρ	Crack tip radius (m)
σ	The remote loading stress (N/m^2)
$\boldsymbol{\sigma_a}$	A parameter of K_{IP} (for sparse cracks)
$\boldsymbol{\sigma_\theta}$	Hoop stress (N/m^2)
$\boldsymbol{\sigma_{ij}}$	Stress at (i, j) (N/m^2)

σ_l	Axial/Longitudinal stress (N/m^2)
σ_{max}	Maximum stress at the crack tip (N/m^2)
σ_0	The stress that existed at the crack tip before the formation of the crack (N/m^2)
σ_p	A parameter of K_{IP}
σ_r	Radial stress (N/m^2)
Δa	Crack length increment (m)
ΔA	The surface area created when a crack propagate by a distance Δa (m^2)
ΔJ	The energy variation necessary to close a crack along a distance Δa (J)
Δu_l	Displacement of node l in radial direction (m)
Δw_l	Crack opening displacement (m)
ζ	The energy release rate (J/m^2)
ζ_I	Energy release rate associated with mode I stress intensity factor (J/m^2)
ζ_{II}	Energy release rate associated with mode II stress intensity factor (J/m^2)
δW	Variation in the work done (J)
$\delta\varepsilon_{ij}$	Variation of the strain at (i, j)
Γ	Integration contour around the crack tip
Ψ	A parameter of R_s

ABBREVIATIONS

AS	Australian Standard.
ASME	American Society of Mechanical Engineers.
CSA	Canadian Standards Association.
CSEM	Chebyshev Spectral Element Method
JIS	Japanese Industrial Standard.
LEFM	Linear Elastic Fracture Mechanics.
LPG	Liquified Petroleum Gas.
LRF	Load Relief Factor.
MMC	Modified Mapping Collocation Technique.
MVCCT	Modified Virtual Crack Closure Technique.
PED	Pressure Equipment Directive.
PET	Polyethylene Terephthalate.
SIF	Stress Intensity Factor.
VCCT	Virtual Crack Closure Technique.

ABSTRACT

The stress intensity factors at the crack tip in an internally pressurized pressure vessel with multiple axial cracks were determined using the energy based modified virtual crack closure technique. This technique was selected because it had been shown to give accurate results in determining stress intensity factors in flat plates despite the fact that only one finite element analysis is required unlike in the virtual crack closure technique which requires two finite element analyses. Furthermore, the literature sources that were consulted did not show evidence of the use of this method in determining stress intensity factors in cylinders with multiple cracks. The Ansys10 Finite Element Analysis software was used to obtain the nodal forces at the crack tip and the nodal displacements in the vicinity of the crack tip. The finite element hoop, radial and axial stresses along the crack face were found to be very close to those obtained using the Lame's equations for an un-cracked cylinder except at the crack tip where a region of stress concentration exist. The stress intensity factors obtained using the modified virtual crack closure technique for cylinders with a single crack were found to be very close to those in literature. However this was after assuming that the crack extends by 37.5% of the length of the finite element behind the crack tip. The same assumption was also found to be valid for cylinders with multiple cracks.

The cylinders that were considered in this analysis were those with $1 \leq n \leq 100$, $0.1 \leq a/t \leq 0.7$ and $1.5 \leq Y \leq 2.5$. Most of the stress intensity factor values obtained for both single crack and multiple crack cases were in good agreement with those found in

literature with the error being less than 5% in most cases. It is anticipated that this work will form a useful reference material for owners of such cylinders, manufacturers, designers and developers of design codes. A lot of light has also been shed on how effectively this technique can be applied to obtain stress intensity factor values in both single and multiply cracked cylinders.

CHAPTER 1

INTRODUCTION

1.1 Overview

A thick-walled cylinder is a pressure vessel whose wall thickness is greater than one tenth of its inner radius [1]. Thick-walled cylinders are used for a variety of applications such as industrial compressed air receivers, domestic hot water storage tanks, diving cylinders, recompression chambers, distillation towers, autoclaves and many other vessels in mining or oil refineries and petrochemical plants. They are also used as nuclear reactor vessels, space ships and submarines, pneumatic and hydraulic reservoirs under pressure, brake reservoirs and storage vessels of liquified gases such as ammonia, chlorine, propane, butane and LPG [2].

In the industrial sector, thick-walled cylinders are designed to operate safely at a specific pressure and temperature. This is technically referred to as the design pressure and design temperature respectively. A cylinder that is inadequately designed to handle high pressure constitutes a very significant safety hazard. The design and certification of pressure vessels is governed by design codes such as the American Society of Mechanical Engineers' Boiler and Pressure Vessel Code in North America [3], the Pressure Equipment Directive of the European Union (PED) [4], Japanese Industrial Standard (JIS) [5], CSA B51 in Canada [6], AS1210 in Australia [7] and other international standards like Lloyd's Germanischer Lloyd [8], Det Norske Veritas [9], Stoomwezen [10] etc.

Pressure vessels can theoretically be almost of any shape, but shapes made of sections of spheres, cylinders and cones are widely employed. More complicated shapes have historically been difficult to analyze for safe operation and are more difficult to construct. Many pressure vessels are made of steel. To manufacture a spherical pressure vessel, forged parts are welded together. Some mechanical properties of steel are improved by forging, but welding can sometimes reduce these desirable properties. In case of welding, in order to make the pressure vessel meet international safety standards, carefully selected steel with a high impact and corrosion resistance should be used. Furthermore, the correct welding rods should be selected for the particular grade of steel being used and the welding should be carried out by qualified personnel so as to ensure that a high quality weld is obtained [11]. Some pressure vessels are made of wound carbon fibre held in place with a polymer due to the very high tensile strength of the carbon fibre. These vessels can be very light but are difficult to manufacture. Other common materials include polymers such as polyethylene terephthalate (PET) and metals such as copper in plumbing [2].

1.2 Cracks in thick-walled cylinders

In a thick-walled pressure vessel, sites for crack initiation are either caused by design features such as notches, or by accident, e.g, flaws due to manufacturing process or handling. Cracks may also be formed in pressure vessels subjected to extreme loading conditions [12]. The length of a crack in a pressure vessel may increase due to

the application of repeated loads or due to a combination of loads and environmental attack. As its length increases, so does the stress concentration induced by it [13]. Due to the presence of the crack, the residual strength of the pressure vessel decreases progressively with increasing crack size until it becomes so low that the pressure vessel cannot withstand high pressures. Even if the cylinder is not subjected to very high pressures, the crack will continue to grow until the residual strength becomes so low that fracture occurs under normal service pressure [13].

Cracks may result in leakage or rupture failures. Failure, when dealing with pressure vessels especially those subjected to very high pressures, can present major safety issues [14]. The potential dangerous results of leaking pressure vessels include suffocation, poisoning, fires, and even explosion. Rupture failures, which may result from leaking pressure vessels, may be even more catastrophic. Such failures may cause large amounts of damage to property and staff. For instance, the Mihama nuclear power plant accident which occurred on 9th August, 2004 caused the death of four (4) people on the spot and seven (7) others were seriously injured. The accident was caused by a sudden rapture of the pipe carrying pressurized water in the secondary circuit of the power station [15].

Service failure of pressure vessels causes very huge financial losses especially where such vessels are being used in aeroplanes, as reactor vessels, storage tanks or in a power plant [13].

1.3 Statement of the problem

The problem of determining stress intensity factors in pressure vessels has been addressed by a number of researchers [16–19]. Most of this research has been done using methods such as the compounding method, force method, displacement extrapolation, J-integral and singularity subtraction technique. The virtual crack closure technique and its modified version (MVCCT) have also been used in determining SIFs but mostly in cracked straight edged components [20]. To the best of the authors knowledge, the MVCCT has not been utilized in determining stress intensity factors in thick-walled cylinders with multiple cracks.

1.4 Objectives of the Research

Main objective

To use the modified virtual crack closure technique to determine the stress intensity factors in an internally pressurized pressure vessel with multiple axial cracks.

Specific objectives

- To apply the technique to determine the stress intensity factors for both shallow and deep cracks.
- To apply the technique to cylinders with different thickness ratios and different number of cracks.

- To compare the results of this technique with the results of other methods by different researchers.

CHAPTER 2

LITERATURE REVIEW

2.1 Overview

By 1992, the stress intensity factors data available consisted of more than 400 values of K_{IP} (the K due to internal pressure, for different crack arrays and for a wide range of crack lengths), as well as more than 200 values of K_{IA} (the negative K due to the compressive residual stress field induced by the autofrettage process for different configurations of crack arrays and various levels of autofrettage) [18]. A detailed analysis of the available data revealed that the documented results could be classified into two categories namely 'sparse crack arrays' and 'dense crack arrays'. For sparse crack arrays both K_{IP} and K_{IA} were directly proportional to the crack length, 'a', but for the dense case, they depended primarily on the inter-crack spacing, 'd', and were practically crack length independent. Furthermore, the inter-crack aspect ratio , a/d, was found to be the sole parameter that determined which of the two categories each case belonged to.

Based on these results, and using least squares approach, stress intensity factor approximate formulae for K_{IP} and K_{IA} for sparse and dense crack arrays were developed by Perl [18]. The expressions were simple but of very good engineering accuracy and are applicable to the whole gamut of existing results. Cylinders with up to 1024 radial cracks were considered. The following expression was suggested for K_{IP} in dense crack arrays ;

$$K_{IP} = F_1(n)\sigma_p\sqrt{\pi.d} \tag{2.1}$$

where;

$$\sigma_p = \frac{2PY^2}{Y^2 - (1 + a/R_i)^2} \tag{2.2}$$

$$F_1(n) = \frac{1}{\sqrt{2\pi}}[1 - \frac{1.5416}{n+1} - \frac{0.05595}{(n+1)^2} + \frac{12.681}{(n+1)^3} - \frac{22.715}{(n+1)^4}] \tag{2.3}$$

and;

a is the crack length.

d is the inter-crack spacing.

n is the number of cracks.

P is the internal pressure.

R_i is the inner radius of the cylinder.

Y is the diameter ratio.

For sparse cracks, the suggested expression was;

$$K_{IP} = F_2(a/d)\sigma_a\sqrt{\pi.a} \tag{2.4}$$

where

$$F_2(a/d) = 1.12[1 - 0.1465(a/d) - 5.128(a/d)^2] \tag{2.5}$$

$$\sigma_a = \frac{2PY^2}{Y^2 - 1} \tag{2.6}$$

Figure 2.1 shows the variation of F_2(a/d) with a/d [18].

In multiple cracked cylinders, the stress intensity factors were found to reduce to a value MK, where M was a function of cylinder geometry, crack length and number of

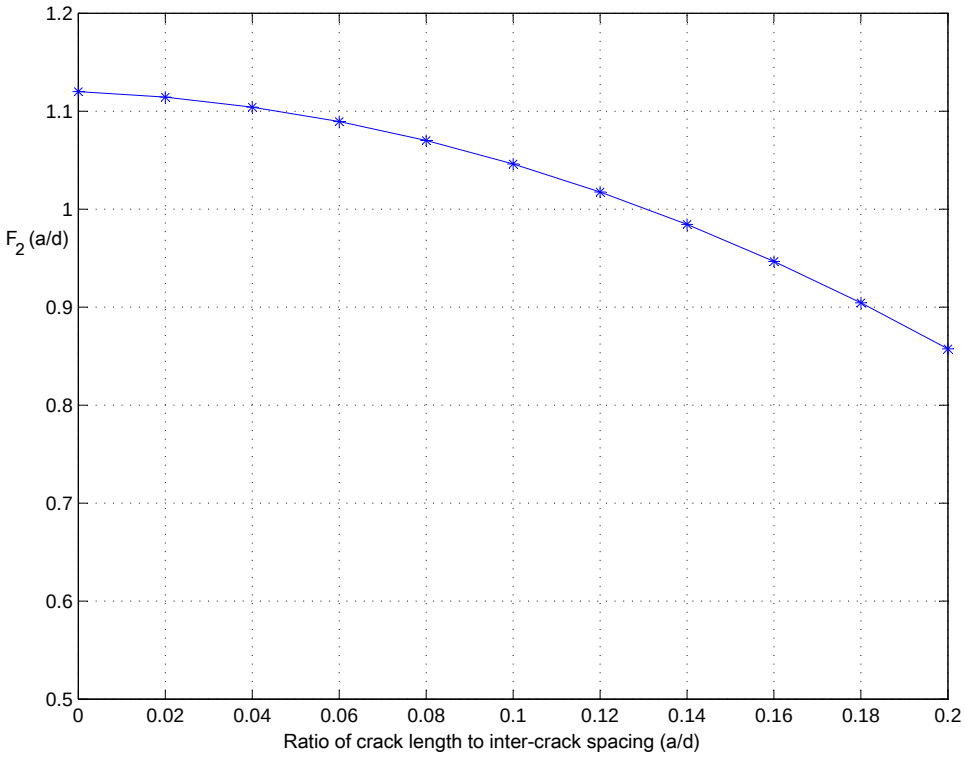

Figure 2.1: Variation of F_2(a/d) with a/d

cracks. Approximate solutions for a tube having diameter ratio of 2 and containing 40 equally spaced cracks (these being characteristics typical of a gun tube) are shown in Figure 2.2. From the figure, it can be seen that multiple cracking affects the stress intensity considerably [21].

Another procedure for estimating stress intensity factor in a thick-walled internally pressurized tube containing internal radial cracks was proposed by Clark and Morton [22]. Its main advantages were its extreme simplicity and ease of application. It surprisingly gave good agreement with other approximations despite the mathematically unjustified assumptions that were made.

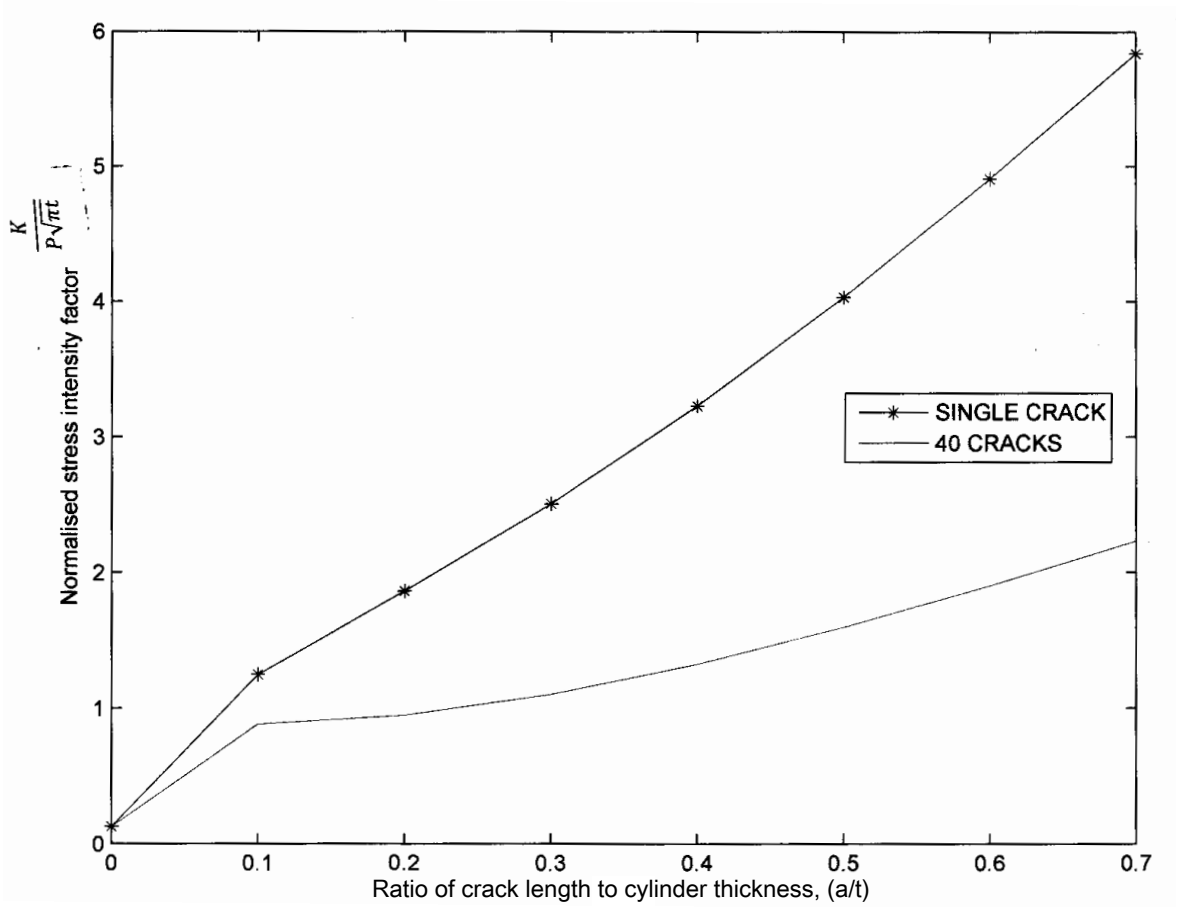

Figure 2.2: Effect of multiple cracks on SIF [21]

The concept of load relief factor was used to determine in an approximate manner, stress intensity factors for a multiply-cracked plane and axisymmetric body [16]. To demonstrate the validity of the method (which utilized known available solutions), it was first shown to conservatively agree within engineering accuracy to the results obtained from a more exact formulation. Stress intensity factors were then found for multiple internal radial cracks in cylinders with $1.5 \leq Y \leq 3.0$, $0 \leq a/t \leq 0.7$ and $2 \leq n \leq 50$. Figure 2.3 shows the results obtained for cylinders of various thickness ratio having 48 cracks.

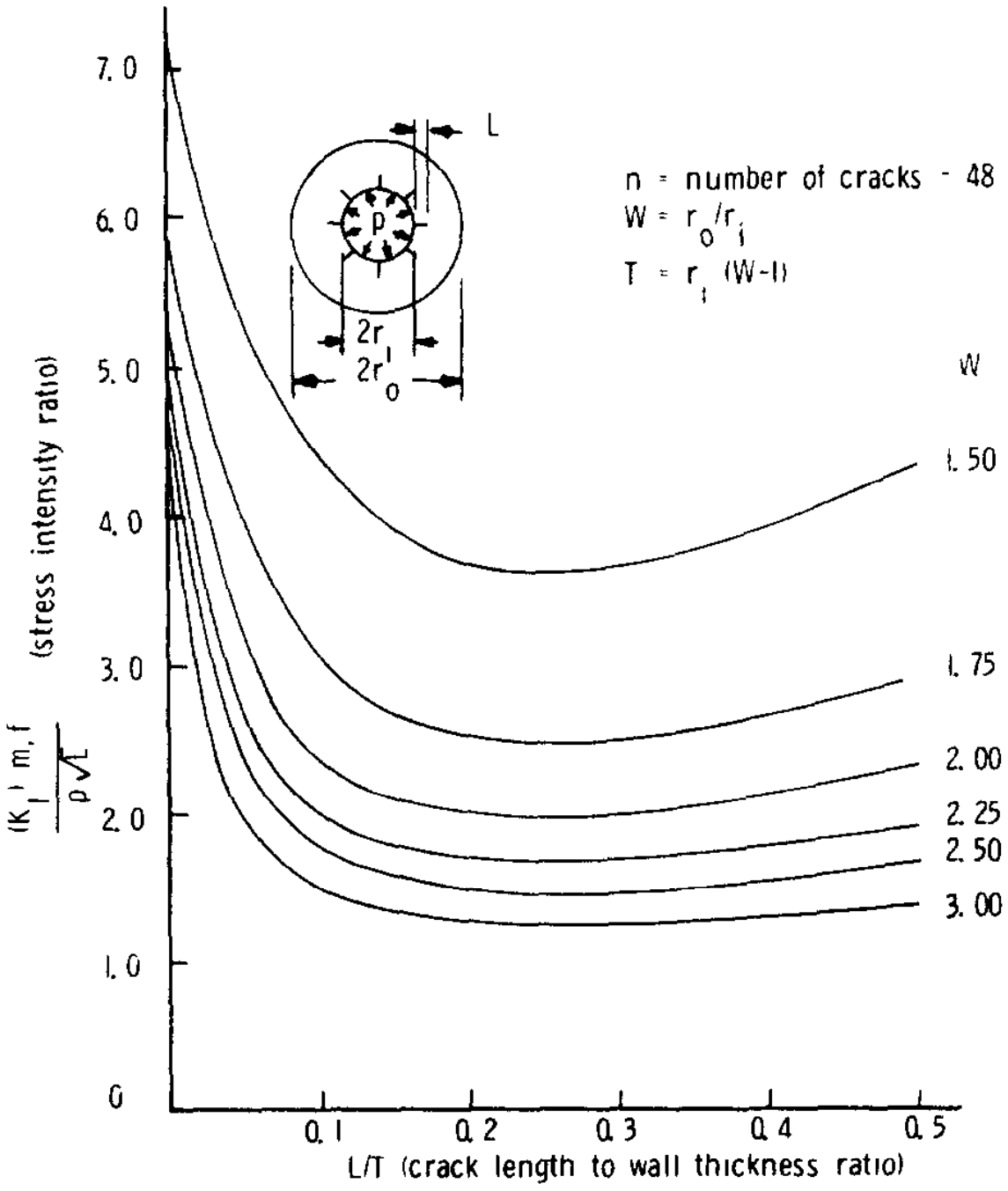

Figure 2.3: K for a multiply cracked cylinder with internal pressure (n=48) [16]

Stress intensity factors were also calculated for a single radial crack in a thick-walled cylinder using finite element technique and compared with those found using a modified

mapping collocation (MMC) technique. Values for two diametrically-opposed cracks in cylinders of Y=1.6 and Y=3.0 were presented, the latter being included since they appeared to represent the worst case of multiple cracking which could occur in vessels of large diameter ratio [23].

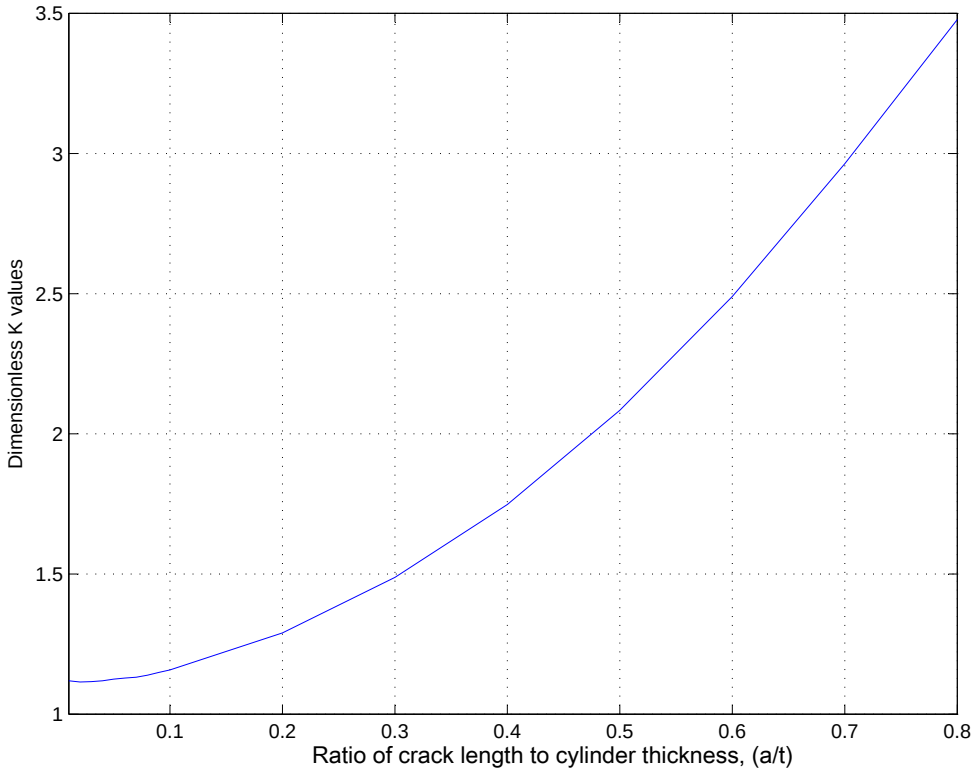

Figure 2.4: K values for two internal radial cracks in a thick cylinder (Y=1.5)

High accuracy mode I stress intensity factors were presented for a wide range of thick cylinders with one or two, internal or external radial cracks. The results were obtained by the use of crack weight functions which were generated via the accurate modified mapping collocation (MMC) method. The cylinders considered were those with $1.5 \leq Y \leq 3.0$ and $0 \leq a/t \leq 0.8$. Figure 2.4 shows the dimensionless K values obtained for a cylinder having a diameter ratio of 1.5 [24]. Comparing the K values

in Figure 2.3 (when Y=1.5 and n=48) with the corresponding values in Figure 2.4 (where Y=1.5 and n=2), it was evident that these values generally increased with a/t in Figure 2.4. However in Figure 2.3, these values decreased with a/t between $0 \leq a/t \leq 0.2$ and then started increasing with a/t when $a/t > 0.25$.

Mode I stress intensity factors were also evaluated for internally pressurized cylinders containing long radial cracks along the internal bore [25]. These factors were calculated for cylinders with $1.25 \leq Y \leq 2.25$, $0.05 \leq a/t \leq 0.5$ and $1 \leq n \leq 40$. Special effort was made to condense the mode I stress intensity factor data into a compact non-dimensional form and to obtain equations which described the effect of diameter ratio and crack depth on these K values. The equations presented were shown to be valid for cylinders with $1.5 \leq Y \leq 3.0$, $0 \leq a/t \leq 0.7$ and $n \leq 512$. For multiply cracked cylinders having internal cracks, the equation for determining mode I stress intensity factor was presented as;

$$K_h = R_N(5.714\alpha^{0.5} - 4.258\alpha + 5.651\alpha^{1.5})P\sqrt{t} \tag{2.7}$$

where;

$$R_N = \frac{1 + B_1\beta^2}{1 + B_2\beta^2} \tag{2.8}$$

$$B_1 = 6.02(n-1)^{0.83} \tag{2.9}$$

$$B_2 = 4.07(n-1)^{1.21} \tag{2.10}$$

$$\beta = \frac{a(Y-1)}{t} \tag{2.11}$$

$$\alpha = \frac{a/t}{Y-1} \tag{2.12}$$

Multiple symmetrical radial internal cracks in thick-walled cylinders have also been studied [26]. The K values due to two kinds of internal pressure and full autofrettage process were calculated for a wide range of crack configuration parameters using finite element analysis. A group of formulae for calculating K values were obtained by means of finite element results. The cylinders considered were those with 1.5≤Y≤3.0, 0.05≤a/t≤0.8 and 1≤n≤ 30. For the general situation the following equation has been proposed for 0.1≤a/t≤0.7, 2≤n≤300 and 1.5≤Y≤3.0.

$$\frac{K_s}{P\sqrt{\pi.a}} = \frac{(C_1 + C_2(a/t)^{0.3} + C_3(a/t)^{1.5})/(\ln Y)^{0.25} + (C_4 + C_5(a/t)^{0.3} + C_6(a/t)^{1.5})/(\ln Y)^{1.2})}{(1+(1/Y)^4)\sqrt{(1.2-(a/t)^2)}} \tag{2.13}$$

Where;

$$C_1 = [0.414 - \frac{39.376}{(n+3)^{0.75}} + \frac{132.563}{(n+3)} - \frac{323.131}{(n+3)^2}]/\sqrt{1+(\frac{1}{n+3})^2} \tag{2.14}$$

$$C_2 = [-0.623 + \frac{76.764}{(n+3)^{0.75}} - \frac{299.969}{(n+3)} + \frac{564.756}{(n+3)^2}]/\sqrt{1+(\frac{1}{n+3})^2} \tag{2.15}$$

$$C_3 = [0.334 - \frac{31.737}{(n+3)^{0.75}} + \frac{108.52}{(n+3)} - \frac{310.298}{(n+3)^2}]/\sqrt{1+(\frac{1}{n+3})^2} \tag{2.16}$$

$$C_4 = [-0.223 + \frac{68.596}{(n+3)^{0.75}} - \frac{150.833}{(n+3)} + \frac{239.095}{(n+3)^2}]/\sqrt{1+(\frac{1}{n+3})^2} \tag{2.17}$$

$$C_5 = [0.402 - \frac{106.676}{(n+3)^{0.75}} - \frac{243.382}{(n+3)} - \frac{418.597}{(n+3)^2}]/\sqrt{1+(\frac{1}{n+3})^2} \tag{2.18}$$

$$C_6 = [-0.218 + \frac{60.035}{(n+3)^{0.75}} - \frac{140.805}{(n+3)} + \frac{282.898}{(n+3)^2}]/\sqrt{1+(\frac{1}{n+3})^2} \tag{2.19}$$

The equations presented above were found to give an error of less than 5% when compared with the finite element results. Due to this high level of accuracy they have

been used by a number of researchers in validating their work.

Stress intensity factors have also been determined for internally pressurized thick walled cylinders with radial cracks of unequal length [17]. A two crack length level model was used. In this model the array of radial cracks was assumed to consist of two sub arrays each of which comprised of cracks of constant depth, though the two subarrays themselves could bear different crack lengths. All cracks were evenly spaced while crack length alternated as shown in Figure 2.5.

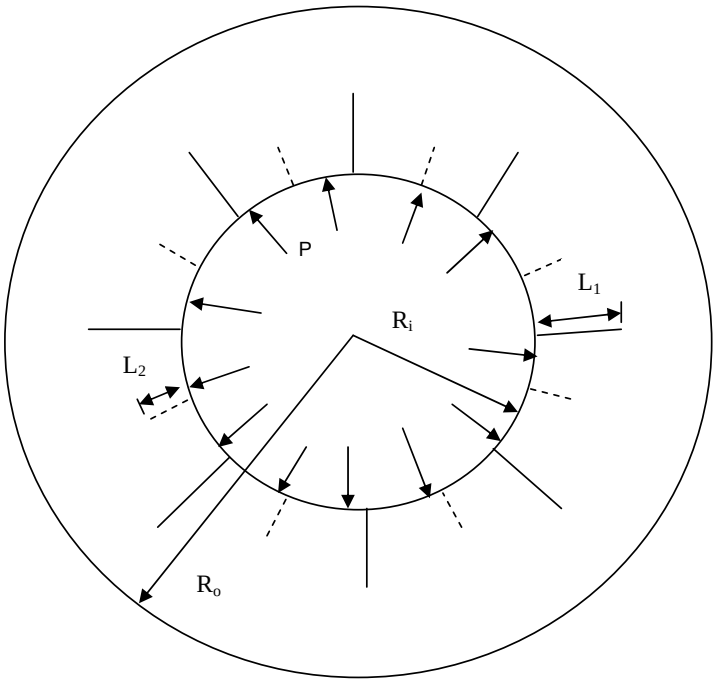

Figure 2.5: A thick-walled cylinder with two subarrays of radial cracks [17]

In Figure 2.5;

$\mathbf{L}_1$ is the crack length for the first subarray (fixed cracks).

$\mathbf{L}_2$ is the crack length for the second subarray (varying cracks).

A few sets of calculations were performed. Within each set the crack length of one subarray was kept constant (the fixed cracks) while the crack length in the other subarray was varied stepwise from case to case (the varying cracks). The results showed that significant interaction between the two types of cracks takes place only within a relatively narrow range of crack length differences. Statistical unevenness of the initial crack lengths would be amplified during the process of fatigue crack growth. The long cracks having a higher rate of growth due to the larger K, would outrun their neighbors, leaving the shorter cracks to drop behind. Each subarray had 64 cracks, Y was 2.0 and $0 \leq a/t \leq 0.25$.

Mode I Stress intensity factor for periodic radial cracks emanating from inner and outer boundaries of an annular ring were evaluated using finite element technique and the concept of cyclic symmetry [27]. Potter's method of solution algorithm was used to reduce the in-core memory requirements. The software and the solution methodology were validated by comparing the results of K for a large number of radial cracks emanating from the inner boundary of the internally pressurized cylinder with those available in the literature. Using the software developed, K was evaluated for two a/R_i ratios and a large number of radials cracks emanating from the outer boundary of a pressurized cylinder. K was also evaluated for a large number of cracks emanating from the inner and outer boundaries of a rotating disc. Further, K was evaluated as a function of a/t for various Y ratios for 4 and 8 cracks emanating from inner and outer boundaries of a rotating disc. Figure 2.6 shows the comparison of the results obtained

with those in literature [27] for a cylinder with up to 95 cracks, Y=2 and a/R_i=0.5.

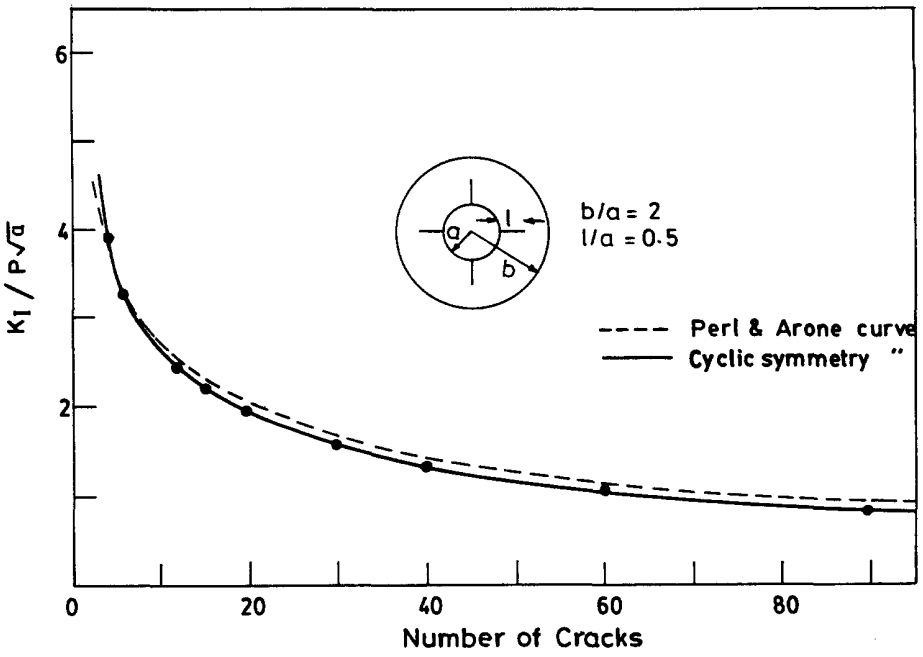

Figure 2.6: Cyclic symmetry results [27]

The variation of K for a single semi-elliptical crack and multiple semi-elliptical cracks which were radial symmetric or unsymmetric array in an internally pressurized thick-walled cylinder was studied by use of 'frozen-stress' photo-elastic method [19]. By means of experimental results and the relative results of other authors, the approximate expression for evaluating K for straight border, semi-circular and semi-elliptical internal surface cracks in thick-walled cylinders were presented. For a radial symmetric array of multiple straight border cracks the equation for K was given as;

$$K_z = R_s K_{s2} \tag{2.20}$$

where

$$R_s = L^{\Psi} \tag{2.21}$$

$$L = 1 - 0.26(a/t) + 0.71(a/t)^2 - 0.9(a/t)^3 + 0.45(a/t)^4 \tag{2.22}$$

$$\Psi = 40[\frac{n-2}{n+7}]^{5/(5(a/t)+2)}(Y-1)^{(14-20(a/t))/25} \tag{2.23}$$

$$K_{S2} = \frac{Y^2}{Y^2-1} J_s P\sqrt{\pi.a} \tag{2.24}$$

$$J_s = 2.29 + 6.1(a/t) + 11.8(a/t)^2 - 6.37Y(a/t) - 6(a/t)^3 - 0.62(a/t)^2Y + 1.1(a/t)Y^2 \tag{2.25}$$

A particular solution for a hollow cylinder with one crack which consisted of two parts has also been evaluated [28]. The first part corresponded to a pair of equal and opposite normal and tangential concentrated forces acting on a crack in an infinite plane region and the second to distributed tractions on both crack surfaces such that the sum of the first and the second part satisfied the prescribed traction boundary conditions on the cracks and cylinder surfaces. The particular solution could be expressed in terms of a density function for each crack giving a system of Fredholm integral equations for multiple crack system. The cylinder shown in Figure 2.7 was analyzed and the results are shown in Figure 2.8.

Mode I stress intensity factors have also been evaluated for large arrays of up to 512 radial cracks emanating from the inner surface of a pressurized thick-walled cylinder [29]. The results obtained are shown in Figure 2.9 where l is crack length, a is internal radius and W is thickness ratio. Furthermore, for cylinders that underwent

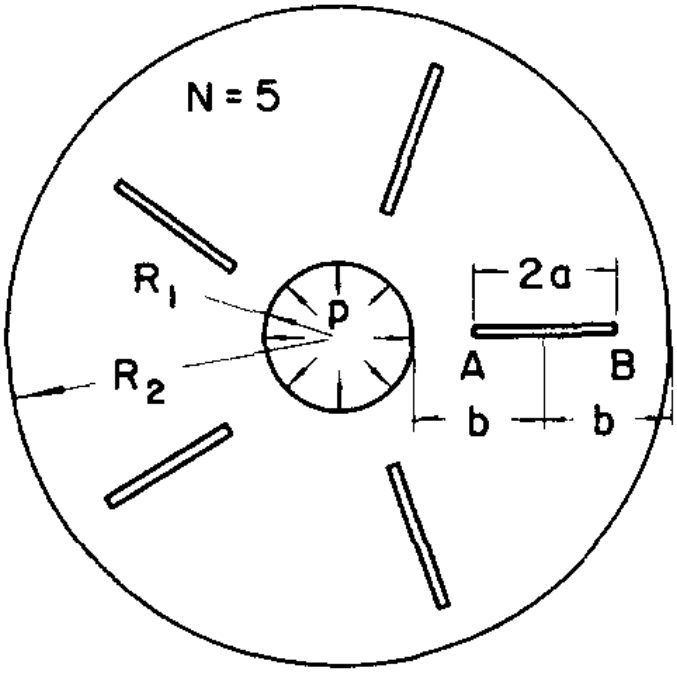

Figure 2.7: Multiple radial cracks [28]

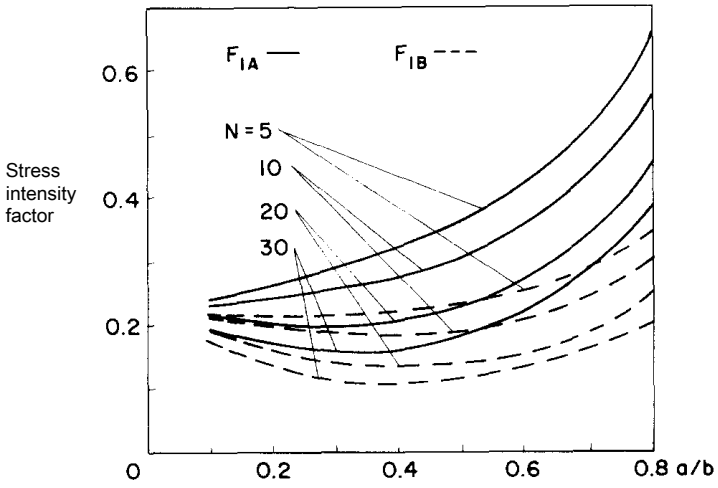

Figure 2.8: Normalized stress intensity factors [28]

autofrettage, the negative K due to the compressive residual stresses were also evaluated. Both positive and negative K values were evaluated, for numerous crack arrays, for a wide range of crack lengths and for a fully autofrettaged cylinder, via the finite element method.

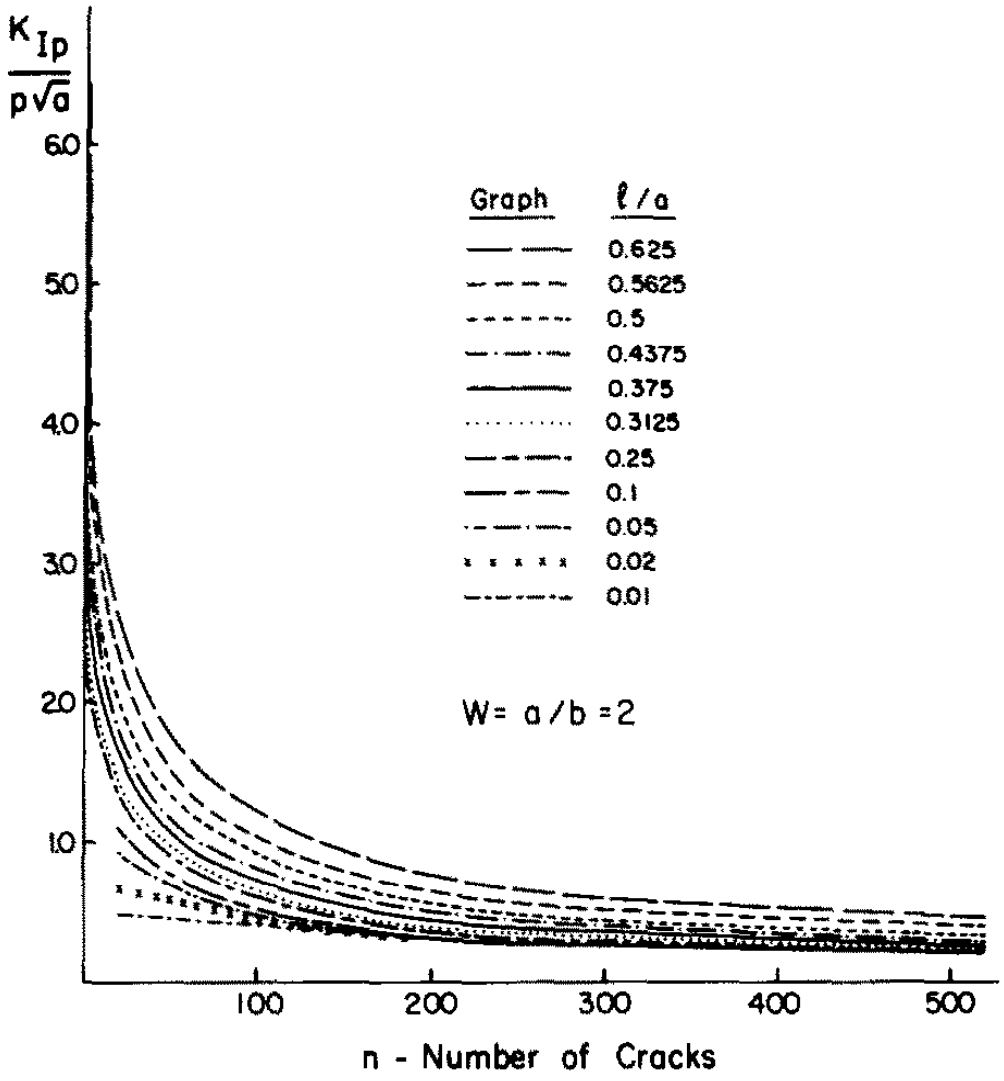

Figure 2.9: K as a function of crack length and the number of cracks [29]

Stress intensity factor influence coefficients have been obtained for a wide range of internal semi-elliptical surface cracks in cylinders with radius ratios 2.0 and 2.5 using the boundary integral equation method for three dimensional elastostatics [30]. Semi-elliptical cracks with an aspect ratio of 0.8 were considered. The crack lengths considered were for $0.2 \leq a/t \leq 0.8$. The influence coefficients obtained corresponded to K_I solutions for the cracks subjected to four different stress distributions, i.e, uniform,

linear, quadratic and cubic pressure variations on the crack faces. These stress distributions can be superimposed to obtain K_I solutions for other stress distributions such as those caused by internal pressure, thermal gradients and autofrettage.

2.2 Areas where MVCCT has been applied successfully

The modified virtual crack closure technique (MVCCT) incorporated with the finite element method was applied to investigate the delamination behavior between stacked copper bumps in 3D chip stacking packaging at package-level and board-level, and the energy release rate at the delamination front was evaluated as the criterion of the crack expansion [31]. The package-level structure was first simulated to validate the dependability of MVCCT and the results revealed that the delamination between copper bumps within specific size would not induce delamination expansion during thermal cycling condition, which showed good agreement with experiment results. The mesh density and the delamination geometry effect analyses were also studied at package-level to ensure the reliable result of finite element analysis. The results showed that the former had an insignificant effect on the energy release rate, while the later had a significant influence. Moreover, based on the simulation results at package-level structure, further delamination behavior at board-level was investigated to predict potential failure mode different from the package-level structure. The results showed higher energy release rate was induced and mixed fracture mode occurred [31].

A general Chebyshev Spectral Element Method (CSEM) for obtaining strain-energy

release rates for crack growth in two-dimensional isotropic materials has also been presented [32]. The procedure used modified virtual crack closure method. This method was developed for different orders of CSEM and suitable expressions for energy release rates were obtained. For a quadrilateral element with four nodes, the expression for mode I strain-energy release rate was found to be similar to Equation 3.24. For a quadrilateral element having nine nodes as shown in Figure 2.10, the mode I strain-energy release rate was obtained as;

$$\zeta_1 = \frac{1}{2\Delta a}[F_{y.j}(U_{y,j-2} - U_{y,(j-2)'}) + F_{y,j+1}(U_{y,j-1} - U_{y,(j-1)'})] \tag{2.26}$$

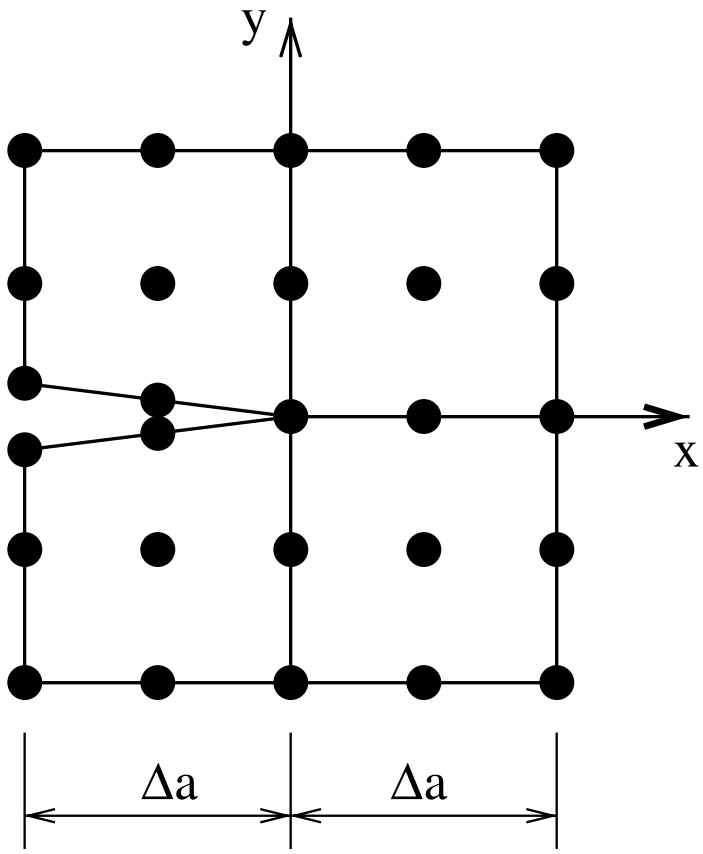

Figure 2.10: Quadrilateral elements with nine nodes [32]

The notation used in Equation 2.26 is illustrated in Figure 2.11. For a pseudospectral

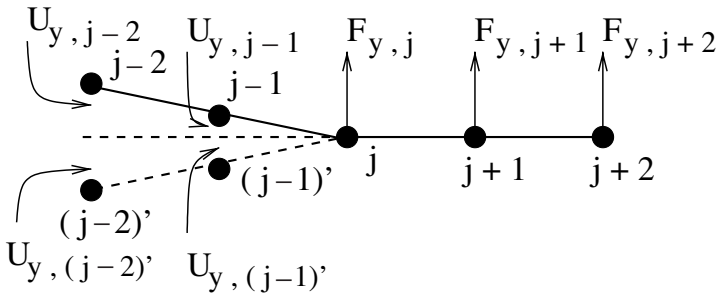

Figure 2.11: Forces and displacement notation for Figure 2.10

finite element mesh near the crack tip shown in Figure 2.12, in which elements with 16 nodes were used, ζ_1 was obtained as;

$$\zeta_1 = \frac{1}{2\Delta a}[F_{y,j}(U_{y,j-3} - U_{y,(j-3)'}) + F_{y,j+1}(U_{y,j-2} - U_{y,(j-2)'}) + F_{y,j+2}(U_{y,j-1} - U_{y,(j-1)'})] \tag{2.27}$$

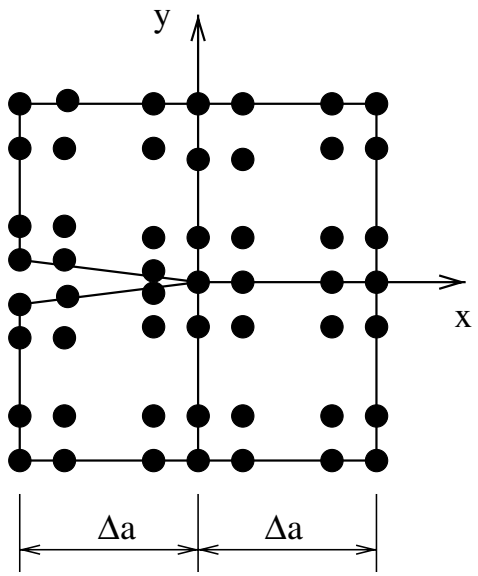

Figure 2.12: Elements with 16 nodes [32]

For a pseudospectral finite element mesh near the crack tip shown in Figure 2.13, in

which elements with 25 nodes were used, ζ_1 was obtained as;

$$\zeta_1 = \frac{1}{2\Delta a}[F_{y,j}(U_{y,j-4} - U_{y,(j-4)'}) + F_{y,j+1}(U_{y,j-3} - U_{y,(j-3)'}) + W] \tag{2.28}$$

where;

$$W = F_{y,j+2}(U_{y,j-2} - U_{y,(j-2)'}) + F_{y,j+3}(U_{y,j-1} - U_{y,(j-1)'}) \tag{2.29}$$

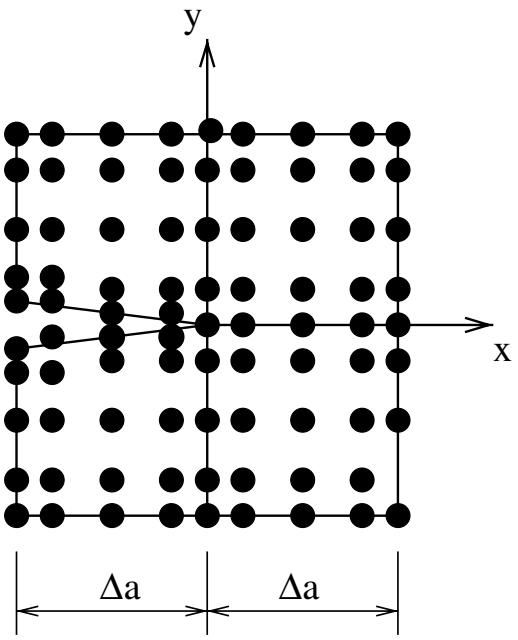

Figure 2.13: Elements with 25 nodes [32]

These expressions for the strain energy release rate were evaluated by applying them to two mode-I and two mixed-mode problems. Two different classes of spectral elements (SEs) were formulated using Chebyshev interpolating functions; the inconsistent conventional SE formulation and the field consistent SE formulation. The convergence was investigated using both formulations. Table 2.1 presents the computed stress intensity factor results from the inconsistent and the consistent finite element formulation and the corresponding percentage error for a/w = 0.5 and a/Δa = 20. The dimensions of a and w are shown in the center-cracked tension (CCT) specimen in Figure 2.14,

which was used in the analysis. The computed results were compared with those of Broek [33]. It was noted from the tabulated results that the error reduced drastically when the order of polynomial was increased i.e. (when the number of nodes in each element was increased). The percentage error reduced from 16.94% to 0.41% as the order of polynomial was increased from 1 to 4 for inconsistent case and from -5.74% to 0.34% for consistent case.

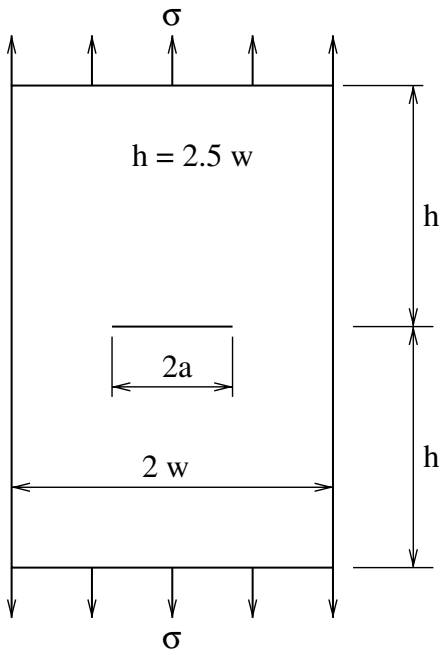

Figure 2.14: Center-cracked tension (CCT) specimen [32]

The effect of crack tip element size was also studied [32]. Table 2.2 shows how reducing the length of the element near the crack tip (Δa) led to a reduction of the error between the reference value [33] and the values of both the consistent and inconsistent formulation. Figure 2.15 shows the single-edge crack (SEC) specimen which was used in this analysis. It was also observed that field consistent formulation always gave better results compared to inconsistent formulation [32].

Table 2.1: Comparison of the convergence of both formulations [32]

Number of nodes in each element	Order of polynomial	Reference value $K_I/\sigma\sqrt{\pi a}$=1.1892 [Broek (1982)]	Inconsistent	% Error	Consistent	% Error
4	1	1.1892	0.9877	16.9442	1.2575	-5.7434
9	2	1.1892	1.1488	3.3972	1.1826	0.5550
16	3	1.1892	1.1767	1.0511	1.1791	0.8493
25	4	1.1892	1.1843	0.4120	1.1851	0.3448

Table 2.2: Effect of crack tip element size on the stress intensity factor [32]

No. of nodes per element	Order of polynomial	a/Δa	Reference value $K_I/\sigma\sqrt{\pi a}$=1.6628 [Broek (1982)]	Inconsistent	% Error	Consistent	% Error
4	1	10	1.6628	1.6087	3.2535	1.6179	2.7003
		15	1.6628	1.6217	2.4717	1.6292	2.0207
		20	1.6628	1.6280	2.0929	1.6348	1.6839
9	2	5	1.6628	1.6306	1.9365	1.6330	1.7922
		8	1.6628	1.6417	1.2689	1.6437	1.1487
		10	1.6628	1.6454	1.0464	1.6473	0.9322
16	3	5	1.6628	1.6442	1.1186	1.6450	1.0705
		8	1.6628	1.6493	0.8119	1.6499	0.7758
		10	1.6628	1.6510	0.7096	1.6515	0.6796
25	4	5	1.6628	1.6494	0.8059	1.6509	0.7157
		8	1.6628	1.6515	0.6796	1.6537	0.5473
		10	1.6628	1.6516	0.6736	1.6541	0.5232

A summary of studies on delamination fracture toughness (critical strain energy release rate) of woven-fabric carbon-epoxy composite specimens by finite element analysis and experiment has also been presented. For finite element analysis, a three dimensional

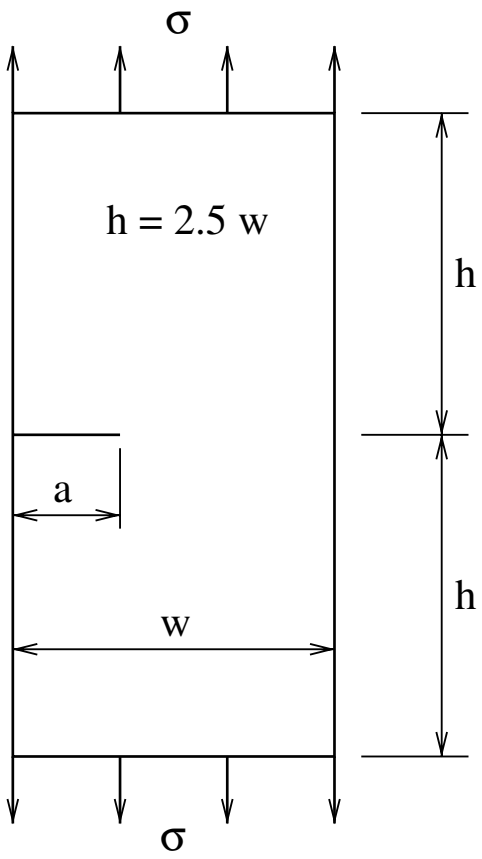

Figure 2.15: Single-edge crack (SEC) specimen [32]

model using plate finite elements was used. The strain energy release rate was computed using the modified virtual crack closure technique. Comparison of mode I critical strain energy release rate values obtained by finite element analysis and experimental results showed a good agreement with a difference of 2.04%. This was illustrated in Table 2.3 in which the average energy release rate obtained using MVCCT was 1.028 whereas the experimental value was 0.986. Comparison of mixed mode (I + II) critical strain energy release rate also showed a fairly good agreement with a difference of 4.1% [34].

Post processing techniques to estimate stress intensity factors using the stress and

Table 2.3: Energy release rate distribution for the specimen [34]

Distance (mm)	G (N/mm)	GI (N/mm)	GII (N/mm)	GIII (N/mm)
1.00	0.959	0.532	0.426	0.0012
3.00	1.028	0.594	0.433	0.0008
5.00	1.046	0.607	0.439	0.0004
7.00	1.052	0.610	0.442	0.0002
9.00	1.054	0.611	0.443	0.0001
11.0	1.054	0.611	0.443	0.0001
13.0	1.052	0.610	0.442	0.0002
15.0	1.046	0.607	0.439	0.0004
17.0	1.028	0.594	0.433	0.0008
19.0	0.959	0.532	0.426	1.162
Average	1.028	0.591	0.436	0.528
Experimental value	0.986	-	-	-

displacement fields calculated by numerical methods have also been reviewed. The techniques that were reviewed are: compounding method, displacement extrapolation method, force method, J-integral, singularity subtraction technique and virtual crack closure method (VCCT) in its classical and modified form. Two benchmark problems were considered to demonstrate the advantages and disadvantages of the analyzed stress intensity factor calculation techniques. The modified virtual crack closure technique proved to be an accurate method for determining stress intensity factors with low computational effort and with good accuracy for common problems [35].

2.3 Conclusion

It was evident that a lot of work had been undertaken as far as the determination of stress intensity factors in thick walled cylinders was concerned. Different researchers have proposed different methods for the determination of these factors in cylinders with

both single and multiple cracks. The modified virtual crack closure technique was also shown to have been applied successfully in a number of areas and it had the advantages of requiring low computational effort and giving good accuracy. However, from the literature sources that were consulted, there was no evidence of the application of this technique in determining these factors in cylinders with multiple cracks. The aim of this work was to employ this method to determine stress intensity factors in these cylinders and compare the results with those obtained using other techniques. It was anticipated that this work would form a useful reference for those interested in methods of determining stress intensity factors and also provide a quick and reliable method of determining these factors in cracked cylinders.

CHAPTER 3

THEORETICAL BACKGROUND

3.1 Stresses in thick-walled cylinders

Stresses in thick-walled cylinders are classified according to the directions in which they act. There are three classes of stresses which are found in a loaded cylinder and these are;

- Hoop or tangential stress, σ_Θ
- Radial stress, σ_r
- Longitudinal/axial stress, σ_l

Any of these stresses at a particular point(R) in a cylinder can be calculated using the Lame's equation. i.e.

$$\sigma_\Theta = A_1 + \frac{A_2}{R^2} \tag{3.1}$$

$$\sigma_r = A_1 - \frac{A_2}{R^2} \tag{3.2}$$

$$\sigma_l = A_1 \tag{3.3}$$

where;

$$A_1 = \frac{P_i R_i^2 - P_o R_o^2}{R_o^2 - R_i^2} \tag{3.4}$$

$$A_2 = \frac{(P_i - P_o) R_o^2 R_i^2}{R_o^2 - R_i^2} \tag{3.5}$$

P_i is the internal pressure acting on the cylinder

P_o is the external pressure acting on the cylinder

R_i is the inner radius of the cylinder

R_o is the outer radius of the cylinder

3.2 Stress concentration factor

The stress concentration factor is the ratio of the greatest stress at the crack tip to the corresponding nominal stress that existed at the location of the crack tip before the formation of the crack. That is;

$$K_f = \frac{\sigma_{max}}{\sigma_0} \tag{3.6}$$

The severity of the stress concentration depends on the geometry of the crack. Designers should therefore always try to reduce stress concentrations as much as possible in order to avoid fatigue problems.

3.3 Stress intensity factor

The stress intensity factor is the linear elastic fracture mechanics parameter that relates remote load, crack size and structural geometry. It predicts very accurately the stress state ('stress intensity') near the tip of a crack caused by a remote load or residual stress. The crack initiation life is highly dependent on the stress concentration

factor K_f value. The crack initiation period is followed by the fatigue crack growth period. For a crack, the K_f value is no longer a meaningful concept to indicate the severity of the stress distribution around the crack tip [36].

The difference between a notch and a crack can be illustrated by considering an elliptical hole. In an infinite sheet loaded in tension, K_f is given by [36];

$$K_f = 1 + 2\sqrt{\frac{a_1}{\rho}} \tag{3.7}$$

$$\rho = b_1^2/a_1 \tag{3.8}$$

where;

a_1 is the major semi-axis of the elliptical hole

b_1 is the minor semi-axis of the elliptical hole

ρ is the tip radius of the elliptical hole

Because a crack is a notch with zero tip radius, K_f would become infinite, and this would be true for any crack length. The stress intensity factor is therefore a better concept of describing the severity of the stress distribution around the crack tip. K can be expressed as;

$$K = \lambda\sigma\sqrt{\pi a} \tag{3.9}$$

where σ is the remote loading stress, 'a' is the crack length and λ is a dimensionless factor which depends on the geometry of the specimen or structural component. The

important feature therefore is that the stress intensity factor fully determines the stress field around the crack tip. Whereas K_f is a ratio, the units for K are $N/m^{1.5}$.

The stress intensity factor is used to determine the fracture toughness of most materials. Fracture toughness is an indication of the amount of stress required to propagate a pre-existing flaw. It is a very important material property since the occurrence of flaws is not completely avoidable in the processing, fabrication or service of a material/component. Flaws may appear as cracks, voids, metallurgical inclusions, weld defects, design discontinuities or some combination thereof. Since engineers can never be totally sure that a material is flawless, it is common practice to assume that a flaw of chosen size will be present in some number of components and use the linear elastic fracture mechanics (LEFM) approach to design critical components. This approach uses the flaw size and features, component geometry, loading conditions and the material property called fracture toughness to evaluate the ability of a component containing flaw to resist fracture.

3.4 Fracture modes

There are three major modes of fracture namely tensile, sliding and tearing mode. These are illustrated in Figure 3.1 to Figure 3.3. Depending on the area of application of a component, fracture can occur in any of these modes or in a combination of any two or all the three modes. Mode I fracture is the condition in which the crack plane is normal to the direction of largest tensile loading. It is the most commonly encountered

mode.

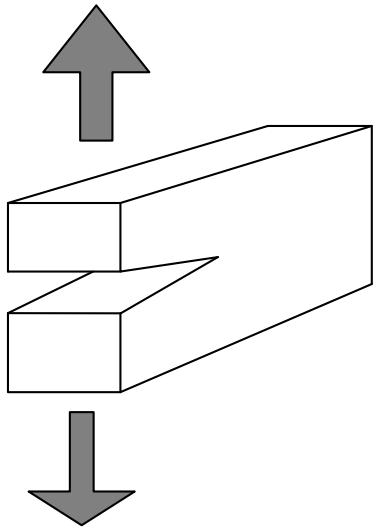

Figure 3.1: Mode I (Tensile mode)

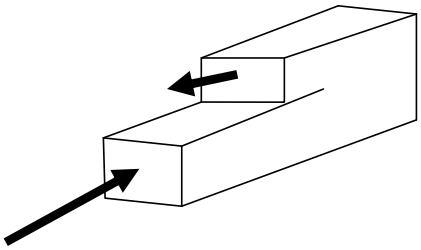

Figure 3.2: Mode II (Sliding mode)

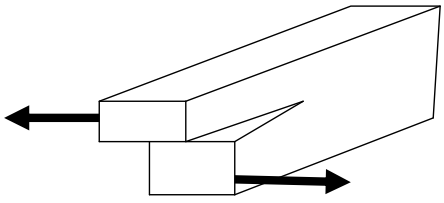

Figure 3.3: Mode III (Tearing mode)

3.5 Methods of determining the stress intensity factor

The stress intensity factors can be calculated using stress and strain analysis or parameters that measure the energy released by crack growth. The estimation of stress intensity factors can be done by analytical or numerical techniques. Normally, the analytical ones are more complex but they have an advantage of applicability for a wide range of crack lengths. For complex structures, it is difficult to perform an analysis taking into account all boundary effects near the crack tip, so the numerical calculation of K has some advantages for these structures. The evolution of computers (hardware and software) permits the use of more complex numerical techniques and to obtain solutions with smaller calculation time. Hence, the numerical techniques for estimating stress intensity factors are nowadays more popular than the analytical techniques.

The following are some of the numerical methods for determining K [35];

3.5.1 Compounding method

This method [37] is used for determining K in complex structures starting from available solutions for simpler solutions. This method consists of decomposing a cracked structure with N boundaries into N ancillary configurations, each one containing one boundary and for which stress intensity factor solutions are available [38].

The stress intensity factor for a structure with N boundaries is given by;

$$K_{1N} = K_0 + \sum_{g=1}^{N}(K_g - K_0) + K_e \tag{3.10}$$

where;

K_0 is the stress intensity factor for the same body without the boundaries.

K_g is the stress intensity factor for the cracked body having only the g-th boundary.

K_e is a stress intensity factor term corresponding to boundary-to-boundary interaction.

3.5.2 Displacement extrapolation

The displacement extrapolation method was developed in order to obtain crack tip singular stresses and stress intensity factors using only nodal displacements of elements around the crack tip [39]. The mode I stress intensity factor is related to the near crack tip displacement as;

$$u_y = \frac{K_I(1+k)}{4\zeta}\sqrt{\frac{r}{2\pi}} \tag{3.11}$$

where;

ζ is the energy release rate.

u_y is the displacement in the y direction (refer to Figure 3.4).

r is a variable distance from the crack tip along the x axis where K can be calculated when r≠0.

$$\kappa = 3 - 4\mu \tag{3.12}$$

in plane stress and

$$\kappa = \frac{3-\mu}{1+\mu} \tag{3.13}$$

in plane strain.

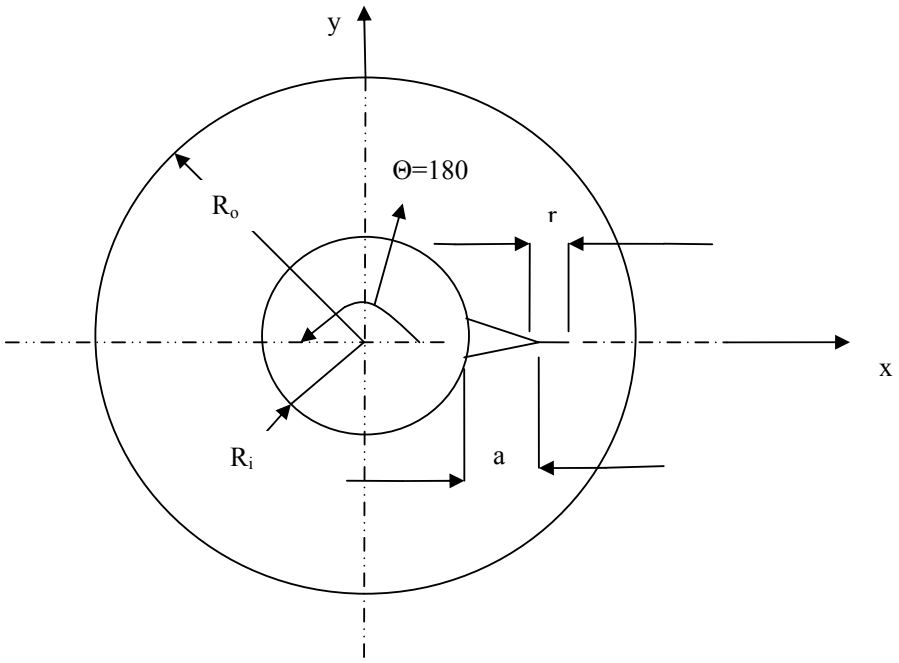

Figure 3.4: Linear extrapolation to r=0 in displacement method

From equations 3.11, 3.12 and 3.13, a relationship between displacements and the apparent stress intensity factor K_0 is obtained and using a linear extrapolation to

r=0, the stress intensity factor at the crack tip can be estimated with a high accuracy.

3.5.3 Force method

The force method is an alternative to displacement method and it uses nodal reactions obtained in a finite element model [40]. The mode I and mode II stress intensity factor values are given by;

$$K_I^{'} = \sqrt{\frac{\pi}{2x_c}} \sum_{i=1}^{n} F_{y,i} \tag{3.14}$$

$$K_{II}^{'} = \sqrt{\frac{\pi}{2x_c}} \sum_{i=1}^{n} F_{x,i} \tag{3.15}$$

where;

x_c is a the distance from the crack tip to a variable location along r.

$F_{x,i}$ and $F_{y,i}$ are forces in x and y direction respectively obtained from the finite element results at various x_c locations.

The value of the stress intensity factor at x_c, i.e K_{x_c}, is calculated at various x_c locations and a linear extrapolation to r=0 is carried out to give the actual stress intensity factor of the structure at the crack tip. The variable distance r is illustrated in Figure 3.4.

3.5.4 J-integral

The J-integral is a contour integral characterizing the strain energy release rate for an elastic non-linear material [41]. The stress field is related to the strain energy density as [42];

$$\sigma_{ij} = \frac{\partial W}{\partial \varepsilon_{ij}} \tag{3.16}$$

where;

σ_{ij} is the stress at (i, j)

∂W is the variation of the work done

ε_{ij} is the variation of the strain at (i, j)

From the definition of potential energy along a contour, work theorem and the previous equation, an integral independent of the integration contour Γ around the crack tip is defined as [42];

$$J = \oint_{\Gamma} (wdb - \mathbf{V}\frac{\partial \mathbf{u}}{\partial x} ds) \tag{3.17}$$

where, w is the strain energy density per unit volume, $\mathbf{V}$ is the traction vector, $\mathbf{u}$ is the displacement vector, ds is the increment of the contour path, x is the crack length direction and b is the direction perpendicular to the crack line. For linear or non-linear elastic materials, the strain energy release rate is equal to the strain energy release rate along a contour at crack tip vicinity i.e, (J=ζ). ζ is related to the stress intensity factor by;

$$\zeta = K^2/E \tag{3.18}$$

in plane stress and;

$$\zeta = K^2/(E/(1-\nu^2)) \tag{3.19}$$

in plane strain.

3.5.5 Virtual crack closure technique

The virtual crack closure technique (VCCT) is based on energy release rate when the crack grows with an infinitesimal increment. It is based on the calculation of the strain energy release rate, using the energy variation when an extension of the crack length is imposed [43].

$$\zeta = \frac{\Delta J}{\Delta a.b} \tag{3.20}$$

where;

Δa is the crack length increment.

b is the thickness of the plate.

For plane strain conditions,

$$\zeta = K^2/(E/(1-\nu^2)) \tag{3.21}$$

This technique requires two finite element analysis in order to calculate the strain energy release rate for a specific crack length. The various ways in which this technique can be applied in the analysis of cracks in components of different geometries have also been shown [44].

3.5.6 Modified virtual crack closure technique (MVCCT)

The modified VCCT is based the same assumptions as VCCT in two steps but in addition it assumes that the conditions at the crack tip are not significantly altered when the crack extends by an increment Δa, from a crack length a+Δa to a length a+2Δa [45]. This implies that the displacements of a region close to the crack tip, when the tip is at specific node, are approximately the same as the displacements at the same location when the tip is at the previous node [35]. Using Figure 3.5 as an example, it is assumed that the displacements at node i will be approximately equal to the displacements at node l when the crack extends from node i to node k.

The energy variation ΔJ necessary to close the crack along a distance Δa is [20]:

$$\Delta J = \frac{1}{2}(X_i.\Delta u_l + Z_i.\Delta w_l) \tag{3.22}$$

where X_i and Z_i are the nodal forces at point i and Δu_l and Δw_l are the node l displacements in radial and circumferential directions respectively.

Therefore the information required for the calculation of the energy variation is obtained from a single finite element analysis. After obtaining the energy variation, the energy release rate is calculated as [20]:

$$\zeta = \frac{\Delta J}{\Delta A} = \frac{\Delta J}{\Delta a.b} \tag{3.23}$$

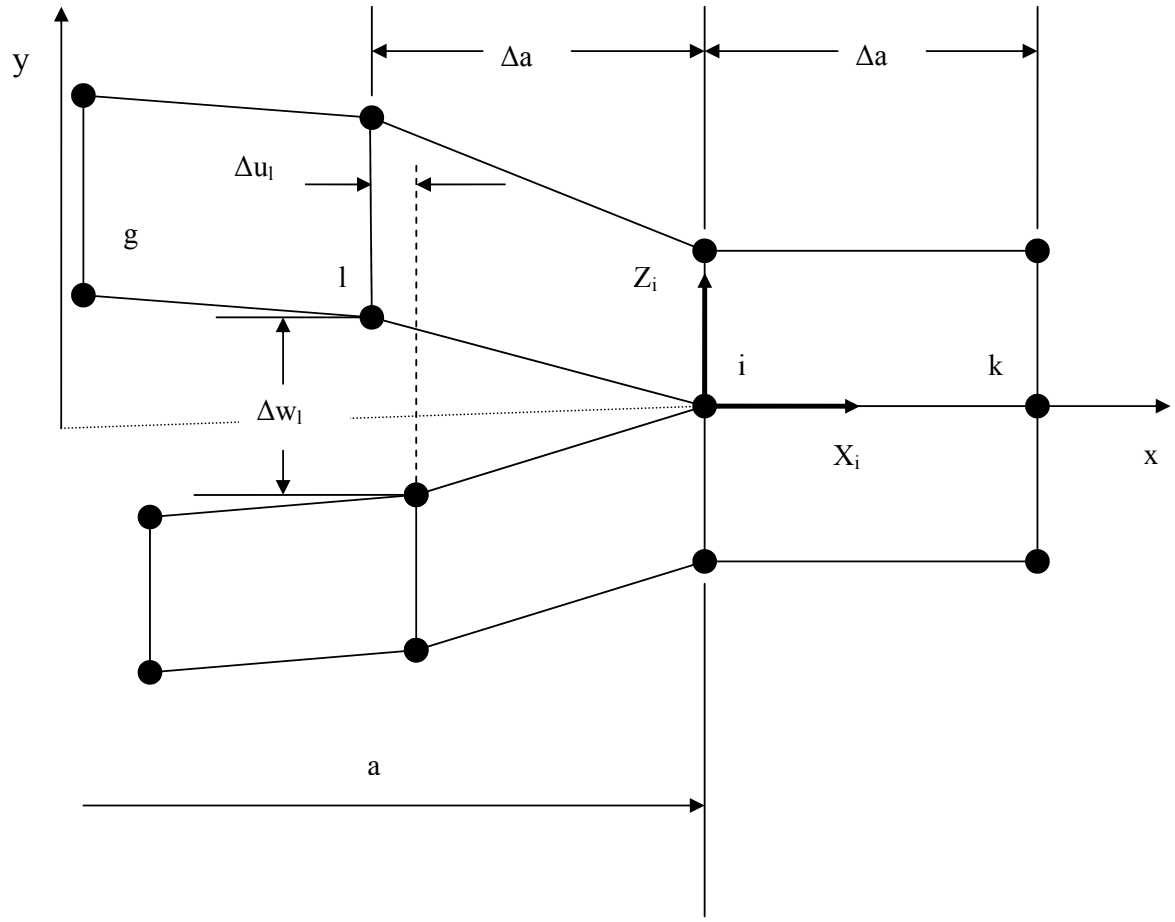

Figure 3.5: Modified VCCT notation

where ΔA is the surface area created by a crack propagation of; in the case of plates with a thickness b, this area is Δa.b .

The calculation of strain energy release rates for each mode is made using the displacements and nodal forces corresponding to the strain energy of that mode. Thus, for the case of Figure 3.5, the energy release rate is [20]:

$$\zeta_I = -\frac{1}{2\Delta a}(Z_i.\Delta w_l) = -\frac{Z_i}{2\Delta a}(w_l - w_{l^*}) \tag{3.24}$$

$$\zeta_{II} = -\frac{1}{2\Delta a}(X_i \cdot \Delta u_l) = -\frac{X_i}{2\Delta a}(u_l - u_{l^*}) \tag{3.25}$$

where;

(u_l, w_l) is the location of node l in the x-y coordinate after the crack extend by a distance Δa.

(u_{l^*}, w_{l^*}) is the location of the node that was originally in contact with node l after the crack extend by a distance Δa.

For the problem being considered in this research the nodal displacement Δu_l is equal to **zero** since there is no relative displacement in radial direction for two points which were originally in contact before the creation of the crack.

CHAPTER 4

METHODOLOGY

4.1 Introduction

The Ansys10 Finite Element Analysis software was used in this study. This software was used to obtain the nodal forces at the crack tip as well as the displacements in the vicinity of the crack tip. These two parameters were then used in the modified virtual crack closure technique to obtain the stress intensity factors. Cylinders with single cracks as well as those with multiple cracks were considered. The following parameters were varied during the analysis of the cylinders:

- The number of cracks. (The variation in number of cracks ultimately led to a variation in the inter-crack spacing).
- The crack length to cylinder thickness ratio (a/t).
- The diameter ratio of the cylinders.

4.2 Single crack analysis

For cylinders with a single crack, the analysis was done by considering one half of the cylinder so as to take advantage of symmetry. Figure 4.1 shows the model that was used but the crack size shown has been exaggerated for the sake of clarity. The model structural properties were chosen as E, (Young's Modulus of Elasticity)=210 GPa and μ, (Poisson's ratio)=0.3. It was then meshed using solid-Tet-10node-187 elements. These elements were chosen because they could be arranged in a regular

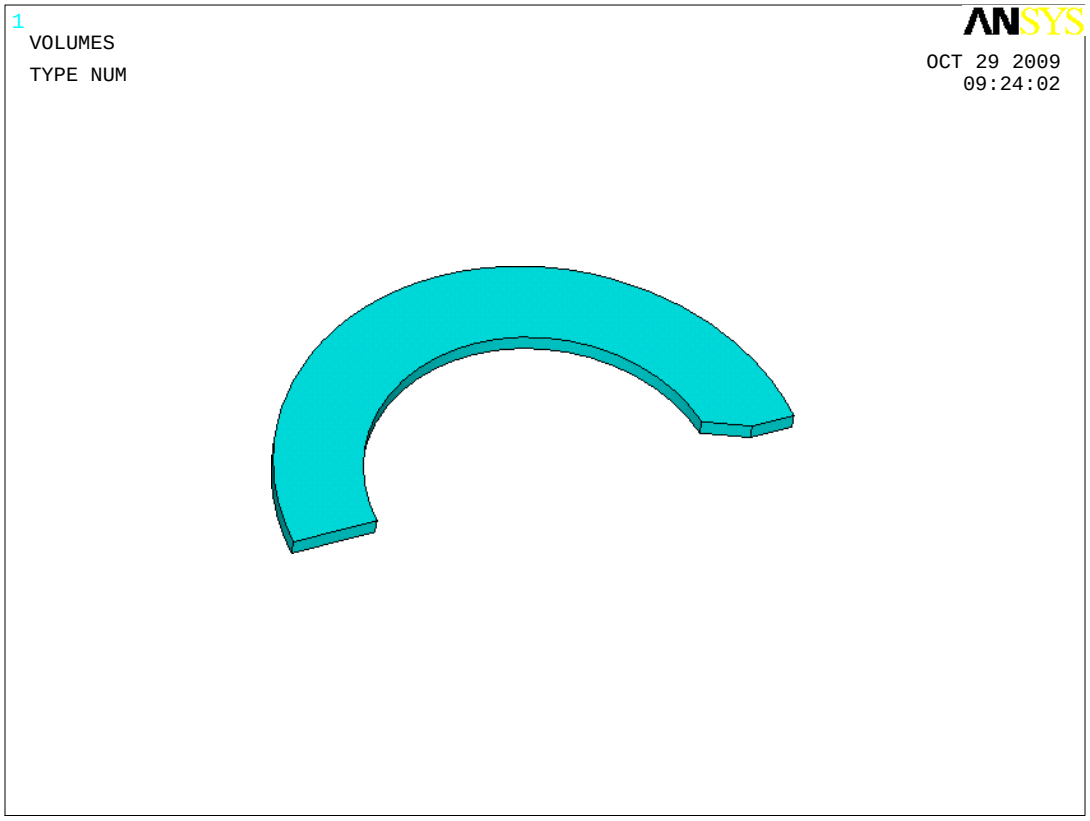

Figure 4.1: 3-D Single crack model

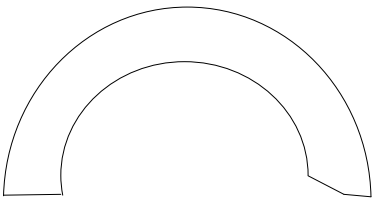

Figure 4.2: Front view of a single crack model

manner around the crack tip and also because they allowed for sufficient mesh refinement around the crack tip.

During the meshing, the model was first freely meshed as shown in Figure 4.3. The meshing of the whole model was then refined as shown in Figure 4.4. Finally mesh

refinement was done at the crack tip and this is illustrated in Figure 4.5.

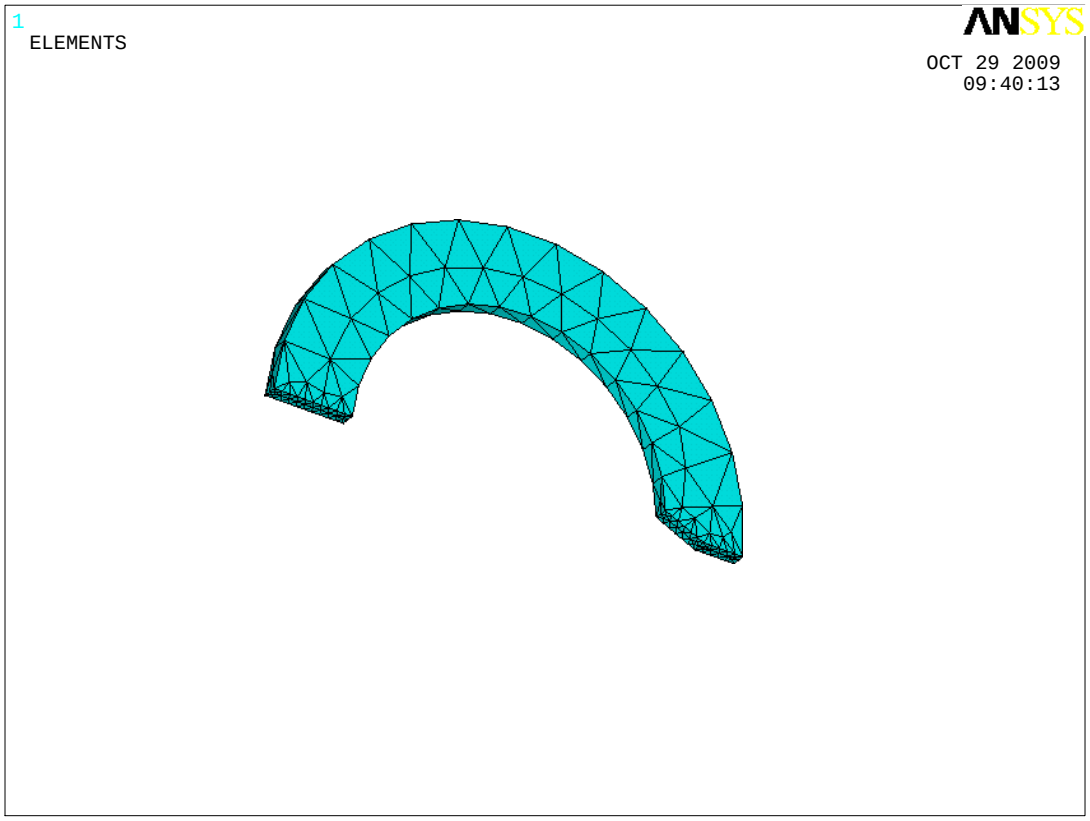

Figure 4.3: Free meshed model

The next stage of the analysis involved the application of boundary conditions. The displacement boundary conditions were applied to prevent the cylinder from rotating about its own axis. The areas in the model were also numbered so as to ensure that the boundary conditions were applied in their appropriate areas. Figure 4.6 shows the model with displacement boundary conditions on area A4 and A7 whereas Figure 4.7 shows the front view of the same model.

Internal pressure was applied on the inner surface of the cylinder as well as on the

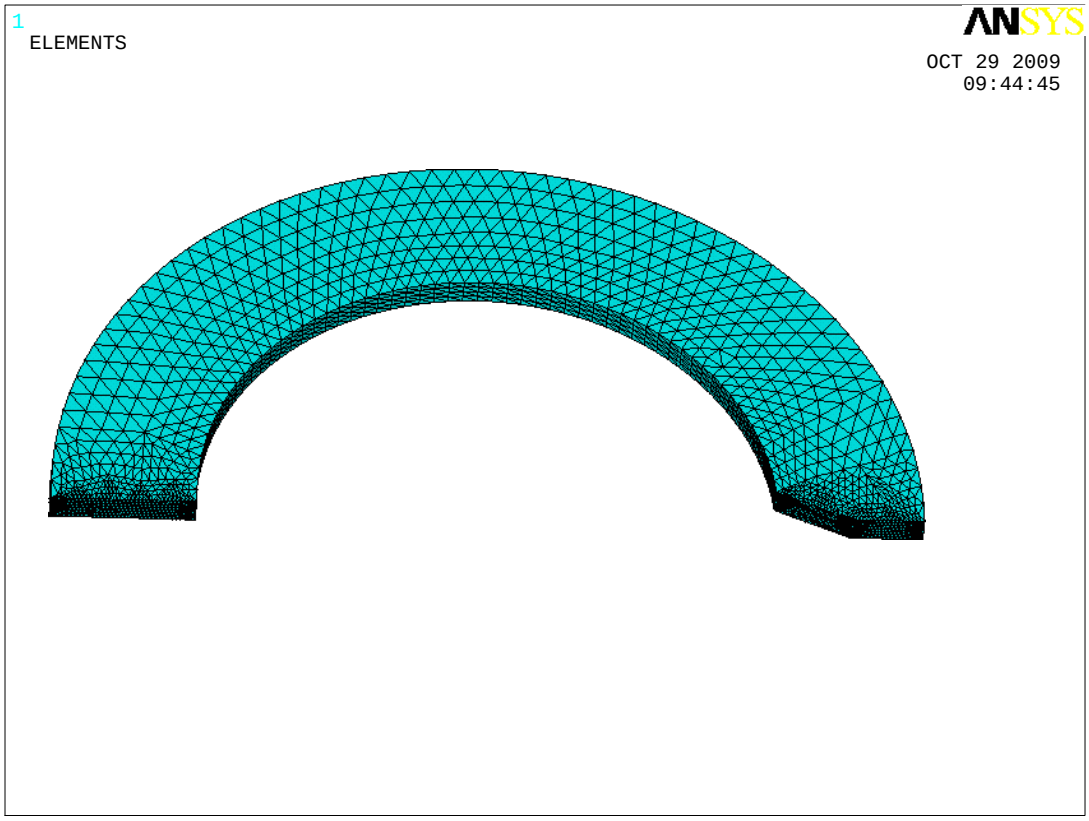

Figure 4.4: Refined meshed model

crack face while making sure that yielding did not occur at any point in the cylinder. The precondition conjugate solver was chosen to carry out the final analysis since it is fast and accurate. Figure 4.8 shows the stress distribution along the crack tip. It is clear from this figure that the stress along the crack tip is higher than the stress at any other point on the cylinder.

After the solution, the deformed and the undeformed model were observed. The maximum stress was also checked so as to verify that it was below the model yield stress. The variation of the radial, hoop and axial stresses was also examined along

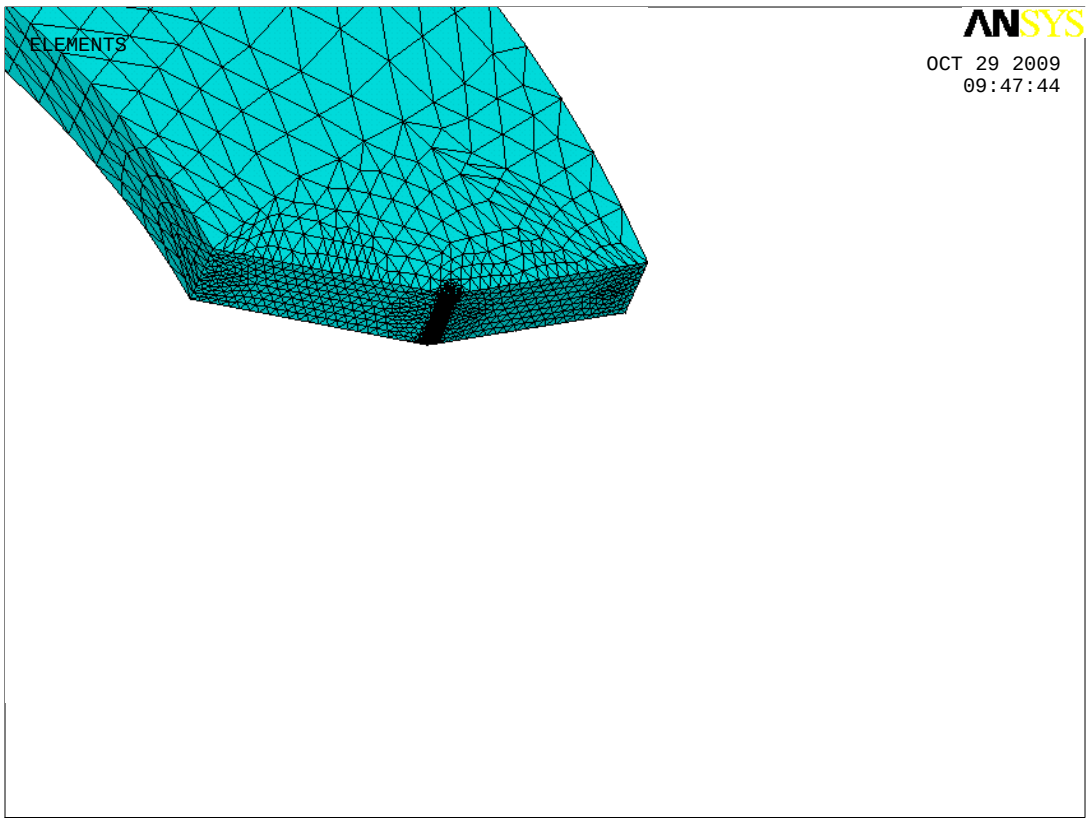

Figure 4.5: Refined mesh at the crack tip

the crack. i.e, the variation of the stresses from the point of crack initiation on the inner surface of the cylinder up to the crack tip. Figure 4.9 shows this variation of stresses from point A to C in Figure 4.10. In Figure 4.9, f is the distance between point A and C in Figure 4.10 whereas e refers to the distances from A to the points where the stresses were recorded. The stresses along the crack were compared to those of a similar flawless cylinder whose stresses were calculated using the Lame's equations. From Figure 4.9 it could be seen that there was no agreement between the finite element stresses and the theoretical stresses and this was because of the pressure applied on the crack face. This pressure introduced a compressive stress on the crack face which reduced the positive hoop stress that is normally present in a flawless cylinder. The

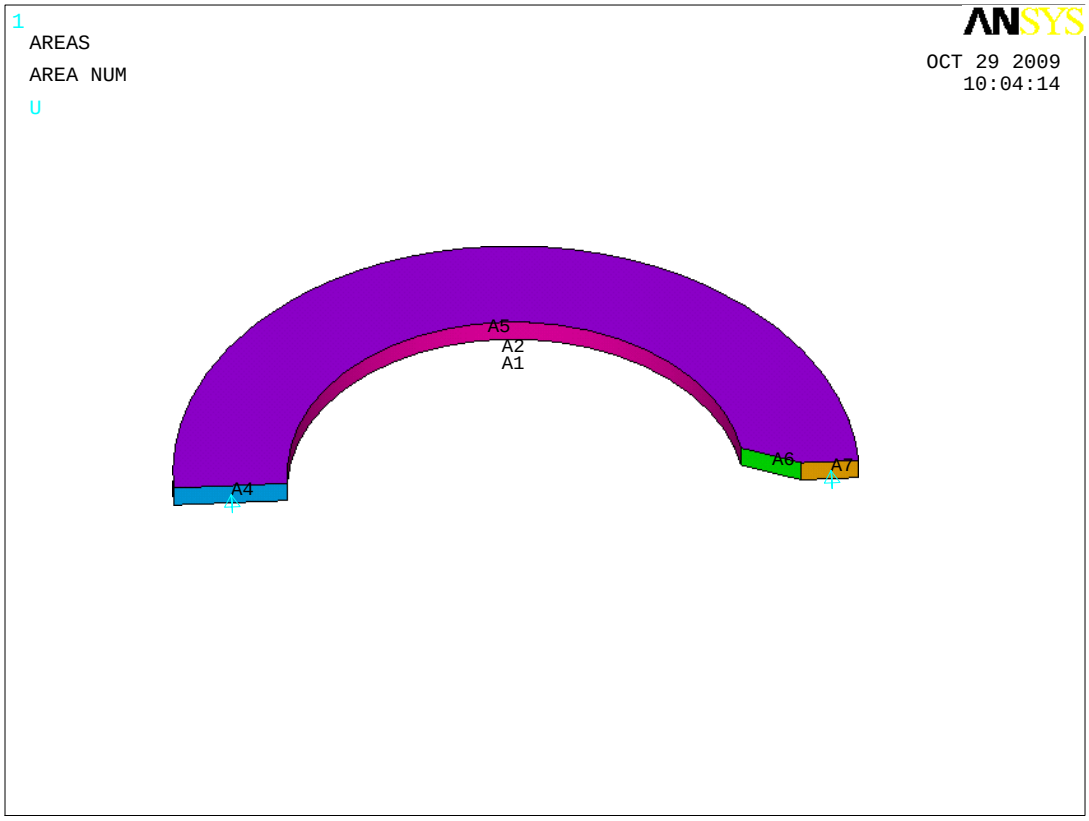

Figure 4.6: Model with boundary conditions

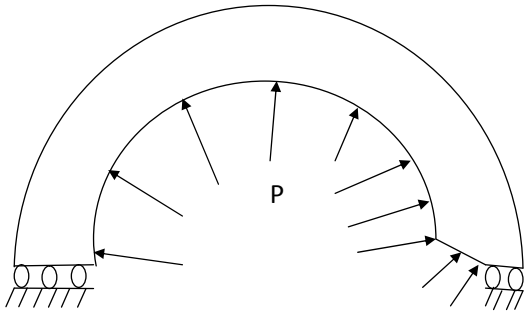

Figure 4.7: Front view of a model with boundary conditions

discontinuity in the cylinder caused by this crack also affected the distribution of both radial and axial stresses. The actual values of both the theoretical and finite element stresses in Figure 4.9 are listed in Table A.1 in the appendix.

The node numbering of the whole model was activated and then a section of the crack

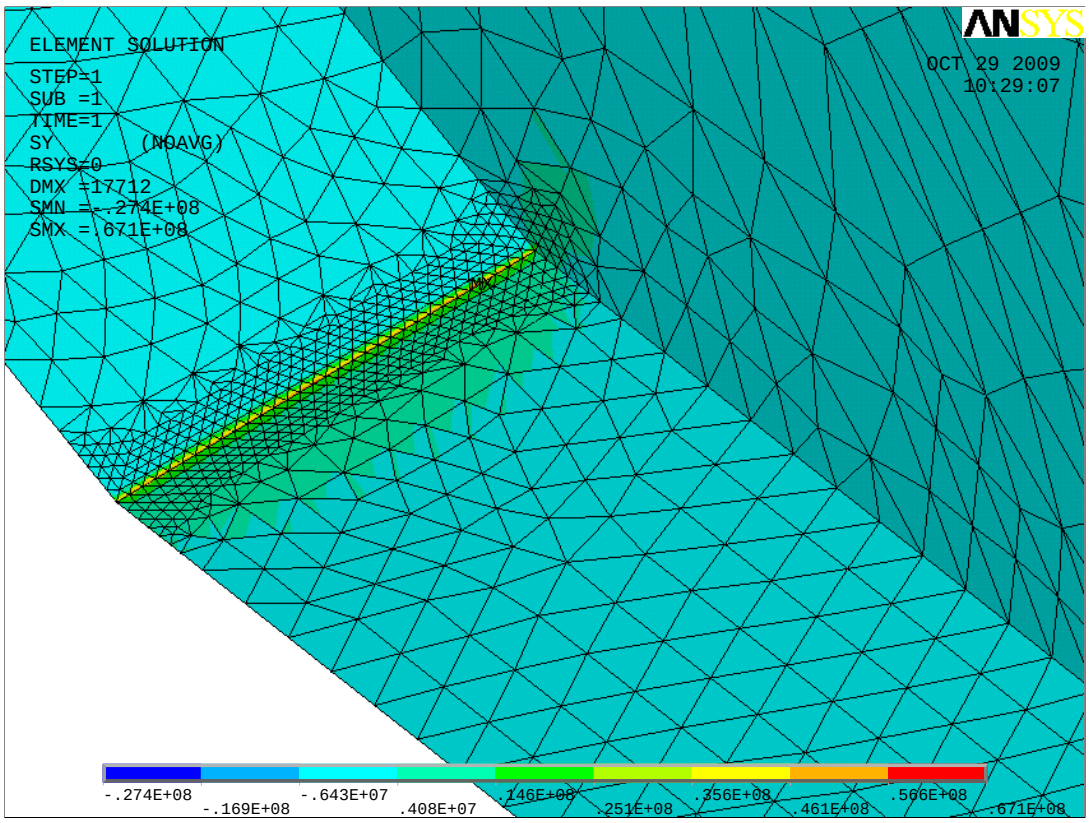

Figure 4.8: Stresses at the crack tip

tip was selected to be used in the analysis. For the selected portion, nodal forces in the hoop/circumferential direction were obtained at five consecutive nodes located along the crack tip. The nodal displacements in the hoop/circumferential direction were also obtained at other five consecutive nodes near the crack tip.

Taking Figure 4.11 as an example, the nodal forces were obtained along the vertical line Q-Q at nodes 53752, 53307, 53297, 53236 and 53209. The nodal displacements were obtained along the vertical line T-T at nodes 54046, 54032, 54083, 54078 and 54077.

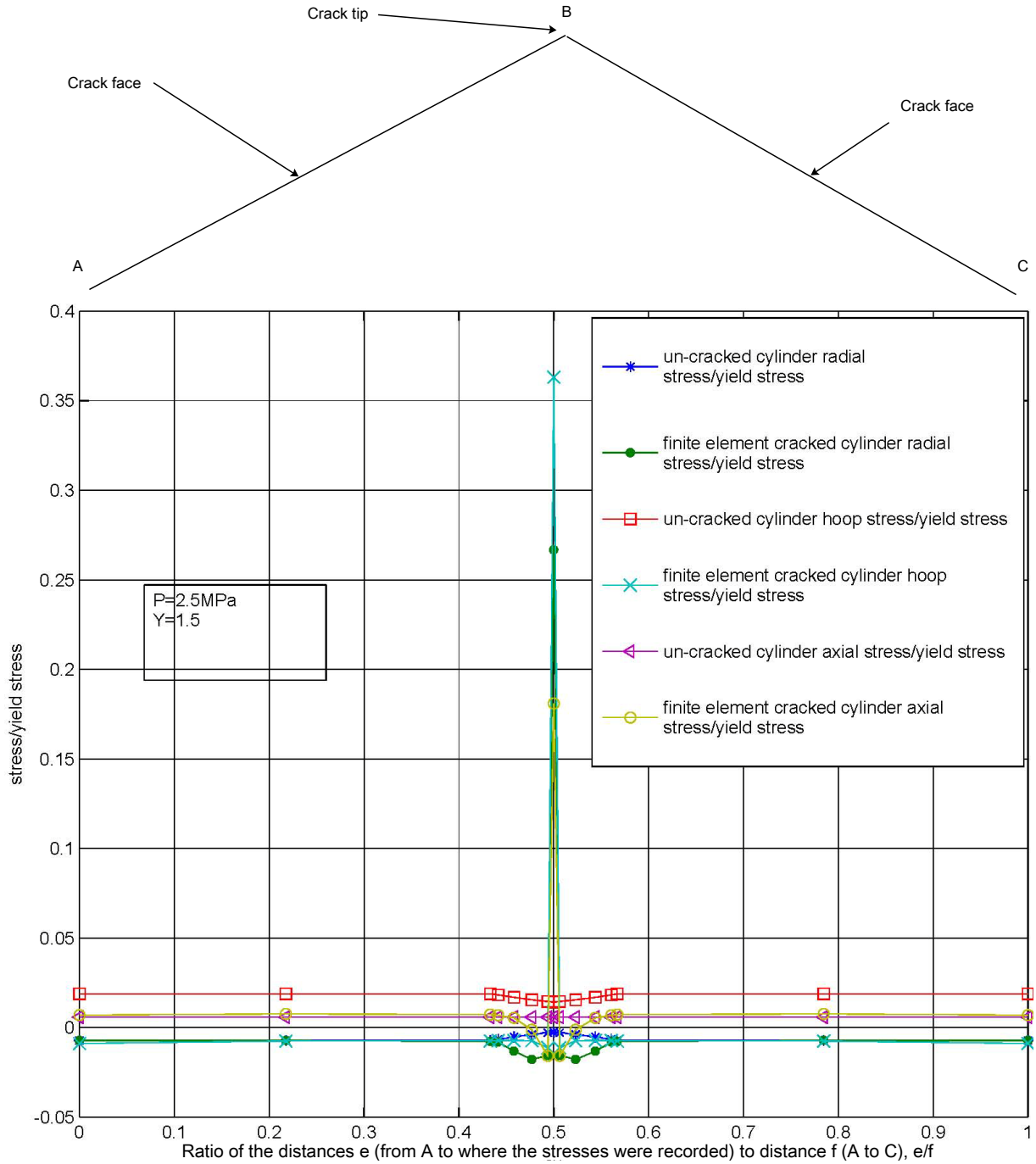

Figure 4.9: Stress variation along the crack

After preliminary investigation, it was found that the modified virtual crack closure technique could not be applied to thick cylinders in the same form as it has previously

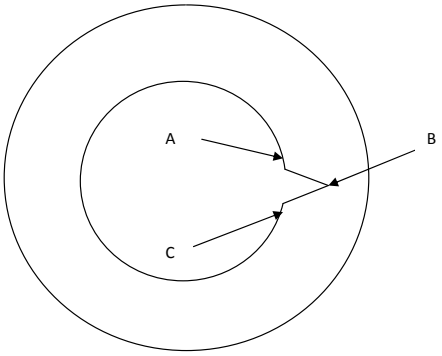

Figure 4.10: Points A to C where stresses were examined

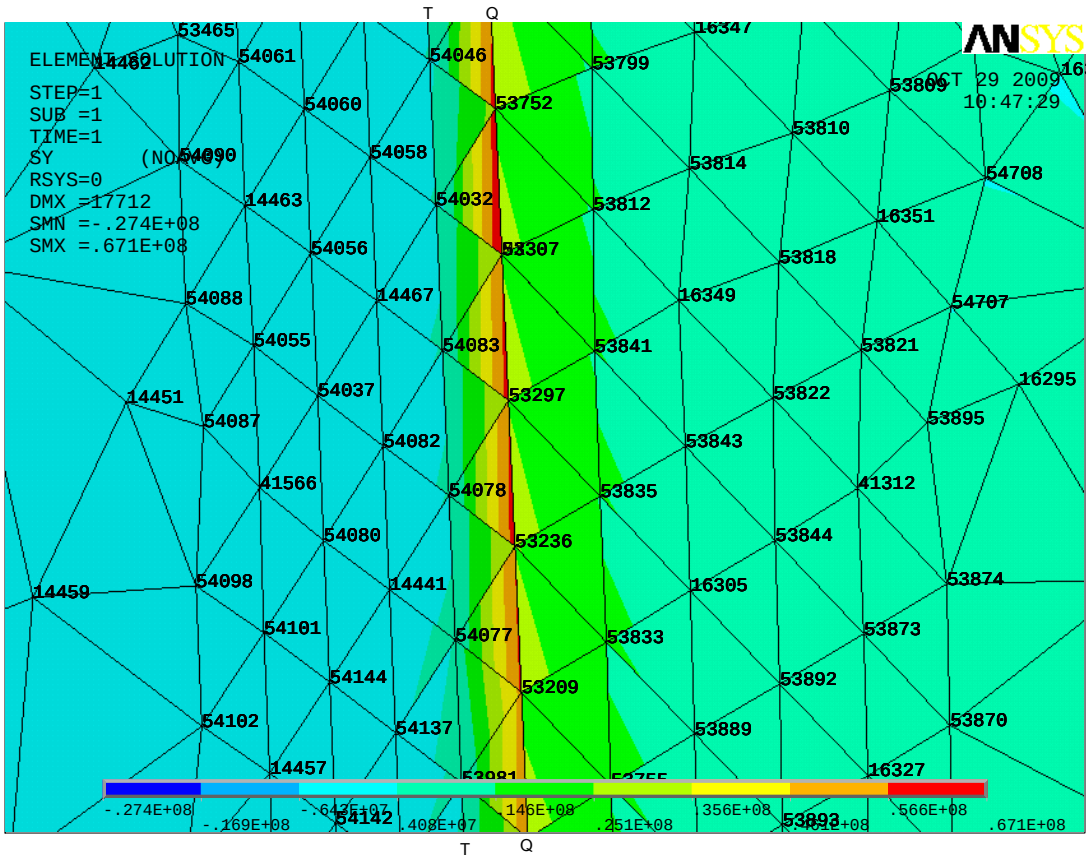

Figure 4.11: Nodes used for analysis

been applied to flat plates. The following expression for K was found to give results which were consistent with those of other researchers.

$$K = \frac{\sqrt{E^*\zeta}}{P\sqrt{\pi.a}} \tag{4.1}$$

where;

$$\zeta = \frac{\sum_{i=1}^{5} Z_i.\Delta w_l}{3m.\Delta a} \tag{4.2}$$

$$E^* = \frac{E}{1-\mu^2} \tag{4.3}$$

E^* is plane strain Young's Modulus of Elasticity.

m is the distance between two consecutive nodes along the crack tip.

Δa is the radial distance from the crack tip to the nodes where the displacement was obtained.

Equation 4.1 was arrived at by making K the subject of the formula in equation 3.21 and putting the following into consideration;

- Whereas equation 3.21 considers a crack of unit width, equation 4.1 considers a portion of the crack width covered by five elements each with an element width equal to m.
- Whereas in equation 3.21 both the element in front of the crack tip and the element behind the crack tip have an equal length of Δa, in equation 4.1, the element in front of the crack tip is assumed to have a length of 37.5%Δa.

For cylinders with a single crack the results obtained were compared with those obtained using equation 2.7.

4.3 Multiple crack analysis

For cylinders with an even number of cracks, due to symmetry, the analysis was done by considering a quadrant of the cylinder. For those with an odd number of cracks, again due to symmetry, the analysis was done by considering a half of the cylinder. Figure 4.12 shows the model that was used in the analysis of a cylinder with three cracks whereas Figure 4.13 show the model that was used for the analysis of a cylinder with six cracks. The lower half of Figure 4.14 shows the part which was ignored in order to take advantage of the symmetry of the cylinder. For the sake of clarity, the sizes of the cracks have been exaggerated.

The procedure for analyzing the cylinders with an even number of cracks is similar to that of analyzing those with an odd number of cracks. In both cases the half crack at the line of symmetry of the model was used for the analysis. The material properties were chosen as E=210GPa and μ=0.3. Solid-Tet-10node-187 elements were used in meshing the models. As an example, the model for a cylinder with six cracks is used to explain how the analysis was done.

The whole model was freely meshed using the selected elements. Mesh refinement was done for the whole model by a factor improvement of three. Finally mesh refinement was done at the crack tip by a factor improvement of two. This is illustrated in Figure 4.15.

All the areas in the model were numbered so as to facilitate accurate application of

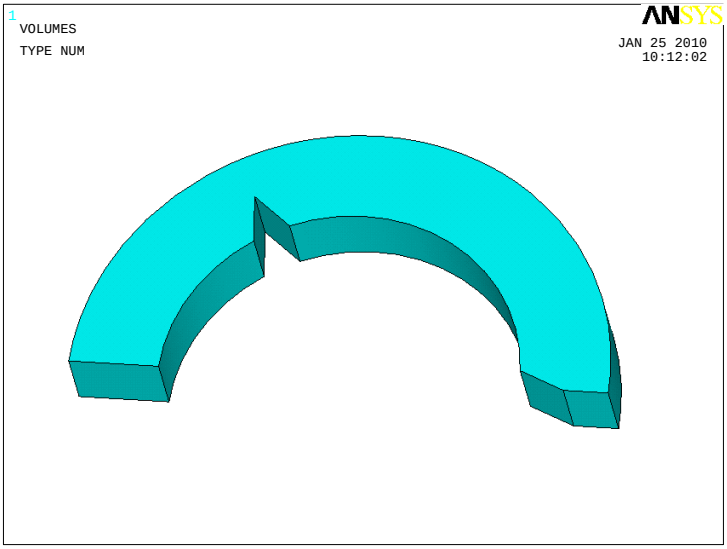

Figure 4.12: 3-D model for a cylinder with 3 cracks

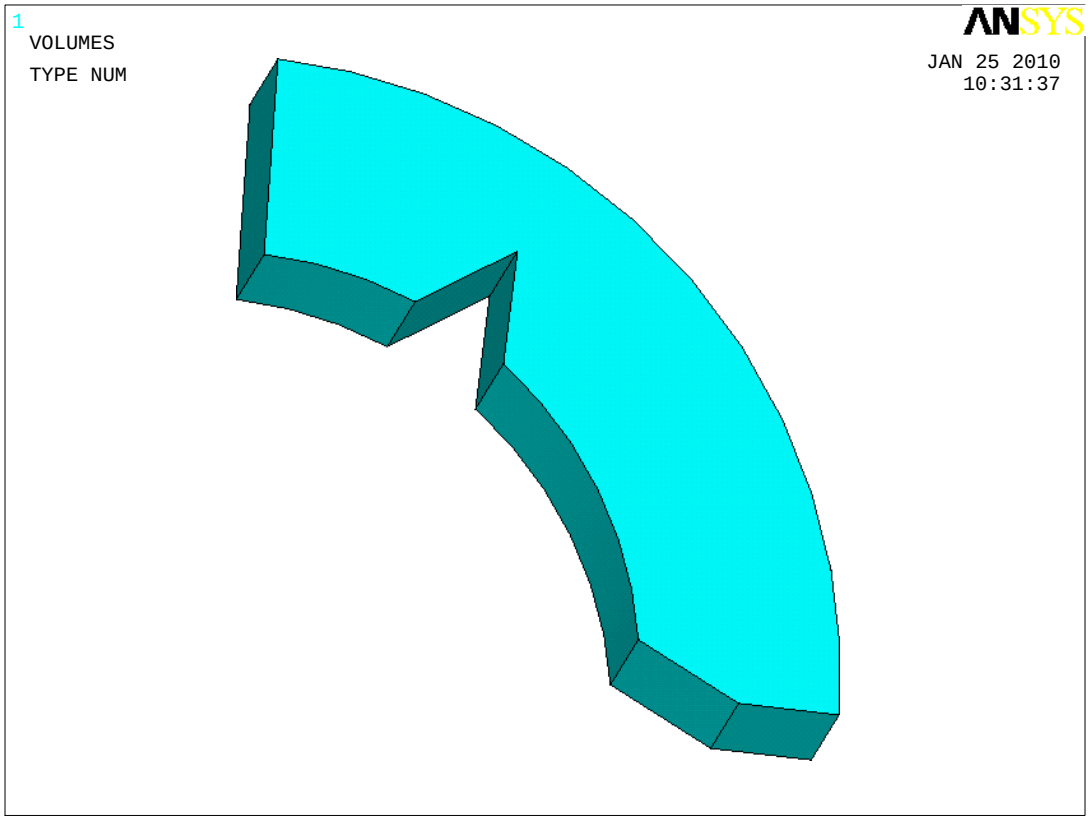

Figure 4.13: Model for a cylinder with 6 cracks

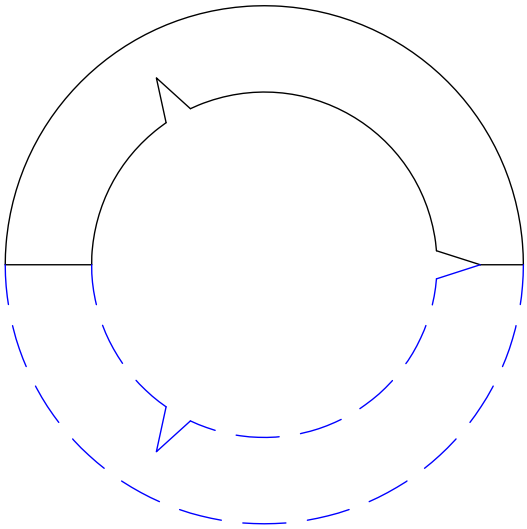

Figure 4.14: Front view of a model for a cylinder with 3 cracks

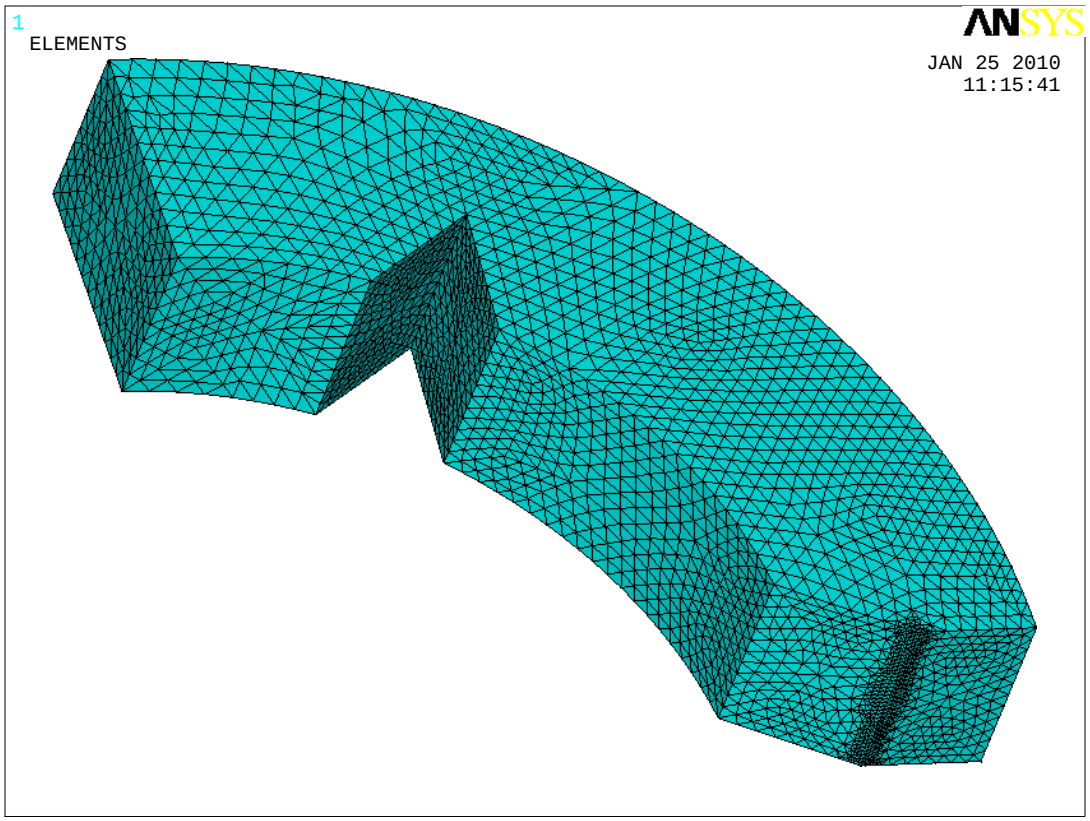

Figure 4.15: Mesh refinement at crack tip

the boundary conditions. Static displacement conditions were applied on both lines of symmetry of the model so as to prevent the rotation of the model after the application of internal pressure. Pressure was applied on the internal surfaces of the cylinder and also on the crack faces making sure that yielding did not occur at any point in the cylinder. Plain strain conditions were assumed for the model which was remote from the cylinder ends. The precondition conjugate solver was then used to obtain the finite element solution for the model.

The node numbering was activated and nodal forces were obtained at five consecutive nodes at the crack tip. Displacements were also obtained at five consecutive nodes near the crack tip and they were used together with the previously obtained nodal forces to calculate the stress intensity factors using equation 4.1. The results obtained for the multiply cracked cylinders were compared with those of Shu [26].

CHAPTER 5

RESULTS AND DISCUSSION

5.1 Model validation

The radial, hoop and axial stresses obtained from the finite element model were compared with their corresponding theoretical stresses obtained using the Lame's equations, i.e, equations 3.1 and 3.2. Figure 5.1 shows the comparison of these stresses for a flawless cylinder with a thickness ratio of Y=1.5. The actual values of the stresses in this figure are listed in Table A.2 in the appendix.

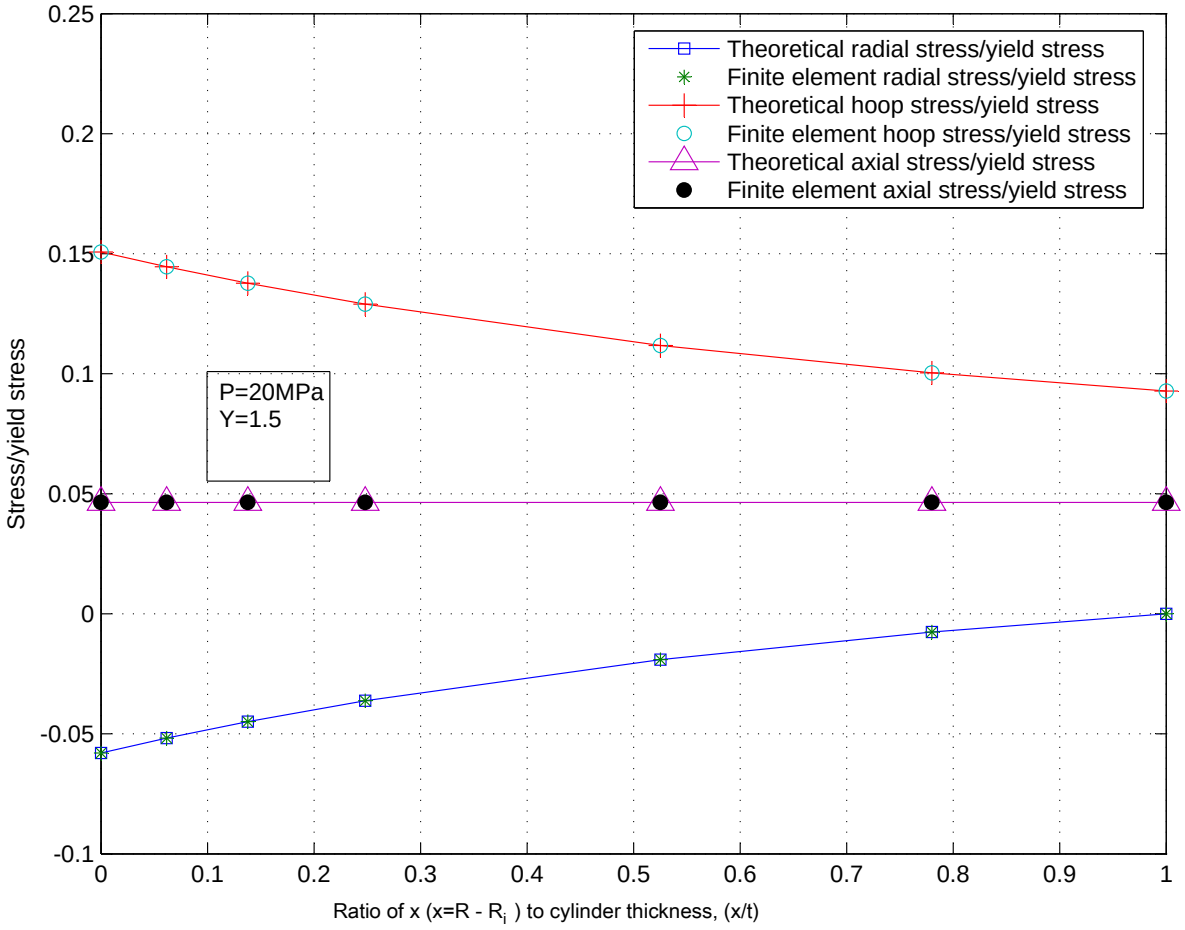

Figure 5.1: Theoretical versus finite element stresses

From the graphs, it was evident that there was very good agreement between the finite element stresses and the theoretical stresses. Both the hoop stress and the radial stress (which has a negative value since it is compressive in nature) were found to decrease with increasing radius of the cylinder. This was because the cylinder considered was subjected to internal pressure only. The axial stresses were found to have a constant value throughout the cylinder thickness and this was the pressure required to counteract the effect of the internal pressure on the cylinder ends. Since there was a good agreement between the flawless cylinder's finite element stresses and theoretical stresses, it was now possible to confidently use the Ansys10 Finite Element Analysis Software to analyze models of cracked thick-walled cylinders.

Figure 5.2 shows the comparison of the finite element stresses with those obtained using the Lame's equations for a cylinder with a thickness ratio of 1.5 having a crack whose length extended up to half the thickness of the cylinder. From the figure, it is clear that the presence of the crack introduced a region of stress concentration at the crack tip where the finite element stresses were very high. The hoop stress at the crack tip was found to be higher than the other stresses at the crack tip and this was due to the fact that the pressure loading on both crack faces was acting in the circumferential direction. This also proved that the cylinder under consideration was more likely to fail in tensile mode and thus showed why the mode I stress intensity factor is of greater interest than the other stress intensity factors.

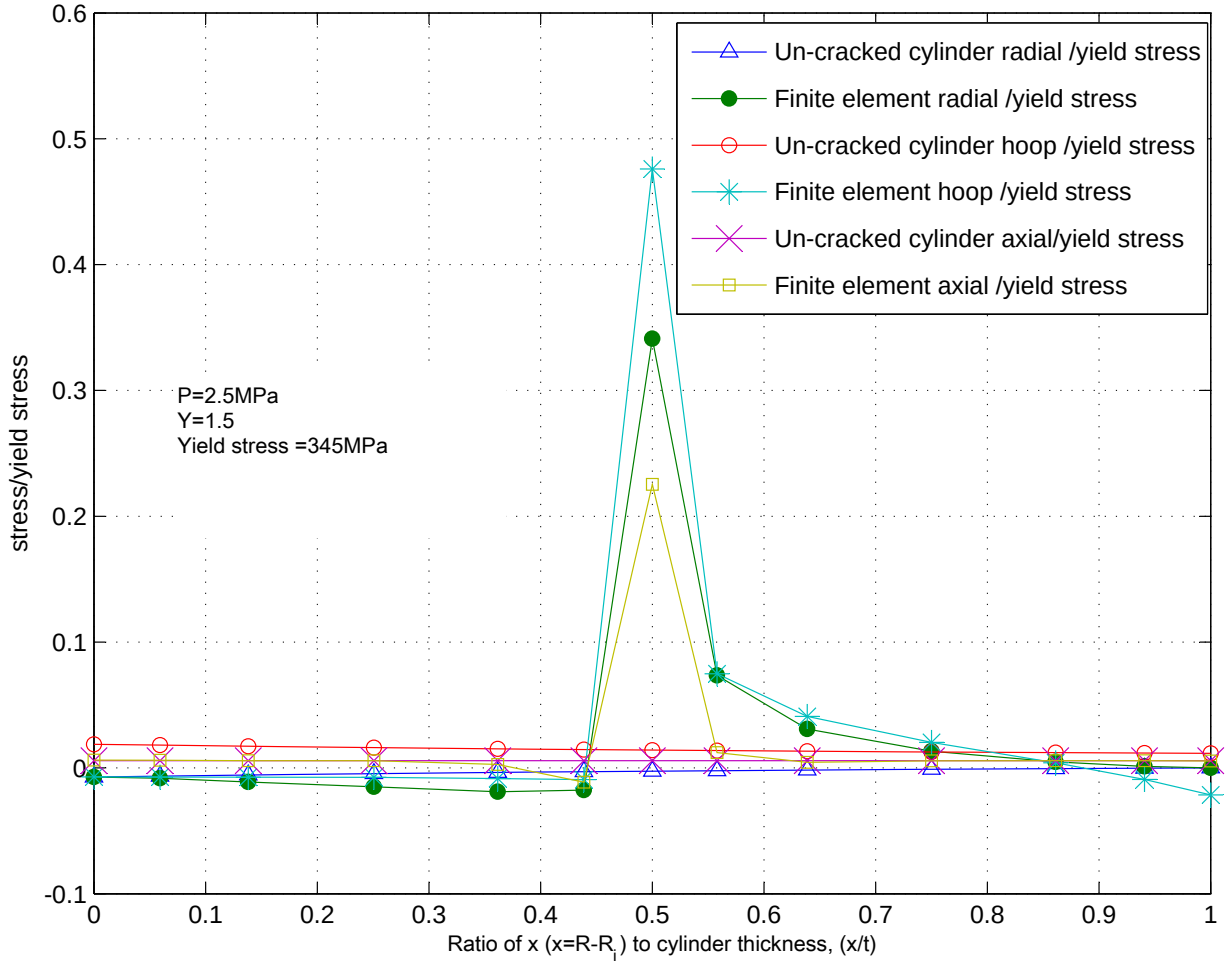

Figure 5.2: A cracked cylinder finite element stresses versus an un-cracked cylinder theoretical stresses

5.2 Application of modified virtual crack closure technique in thick walled cylinders

The modified virtual crack closure technique had earlier been applied in determining stress intensity factors in flat plates subjected to uniform pressure. In thick walled cylinders, the hoop stress that is related to mode I stress intensity factors in radial cracks decreases from the inner surface of the cylinder to the outer surface. Therefore, this method could not be applied in determining stress intensity factors in thick

walled cylinders as it had been applied in determining these factors in flat plates. After preliminary investigations, it was observed that excellent results were obtained after assuming that the crack extends by an amount equal to 37.5% of the length of the element behind the crack tip. Figure 5.3 shows the element in front of the crack tip and the element behind the crack tip whereas Figures 5.4 and 5.5 show how varying the length of the element in front of the crack tip causes K_m to vary from the K_k which was obtained from literature [26]. The actual values of the stress intensity factors in Figure 5.4 and 5.5 are listed in the appendix in Table A.3 and A.4 respectively. All the stress intensity factors presented are dimensionless i.e they have been divided by $P\sqrt{\pi a}$.

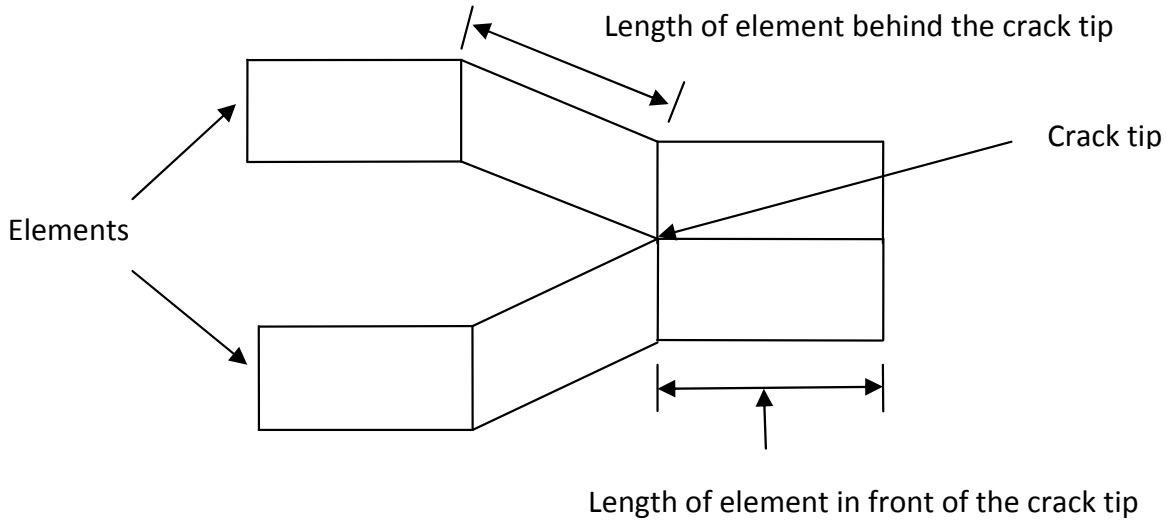

Figure 5.3: Elements behind and in front of the crack tip

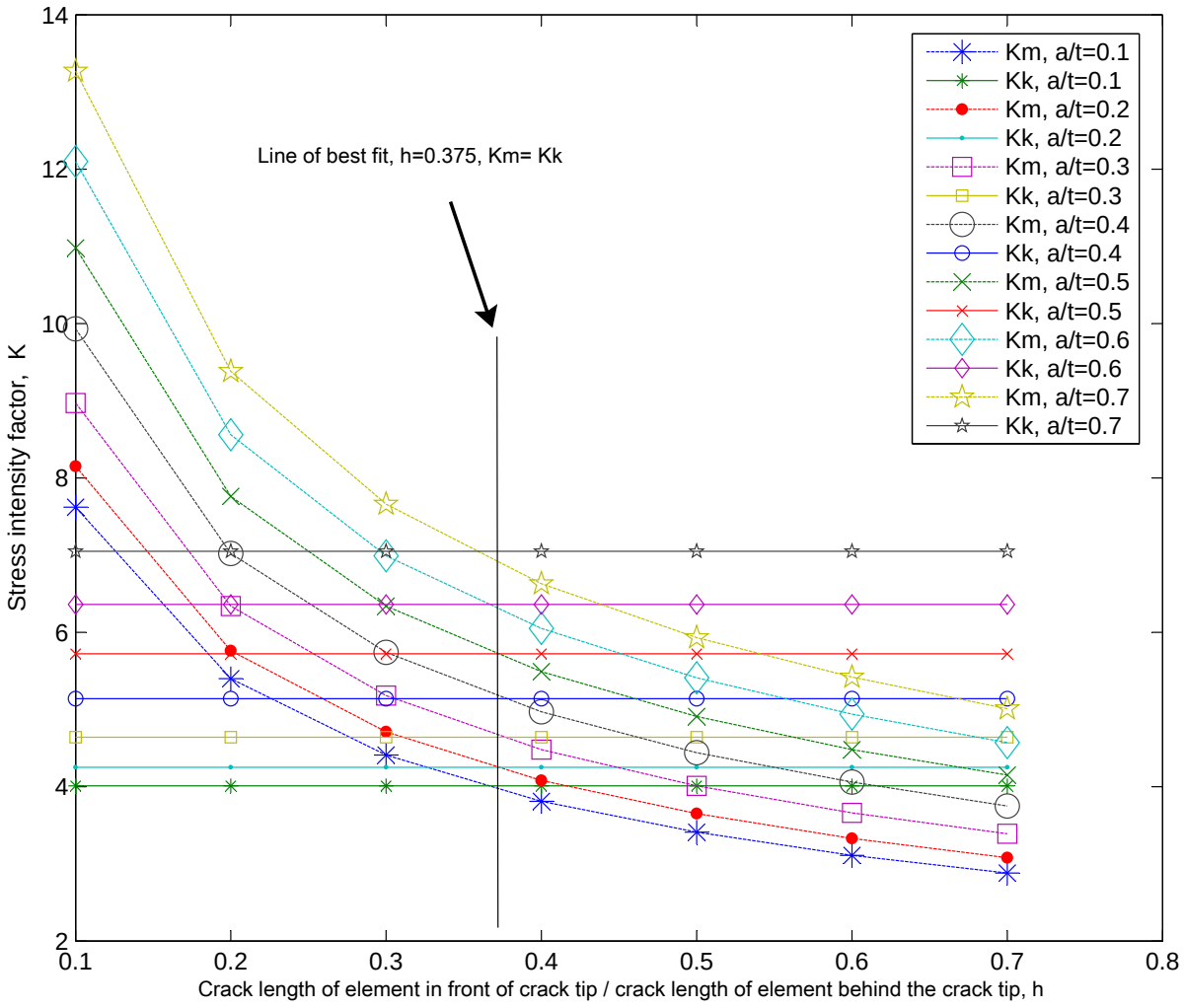

Figure 5.4: Variation of K_m with h for Y=1.5

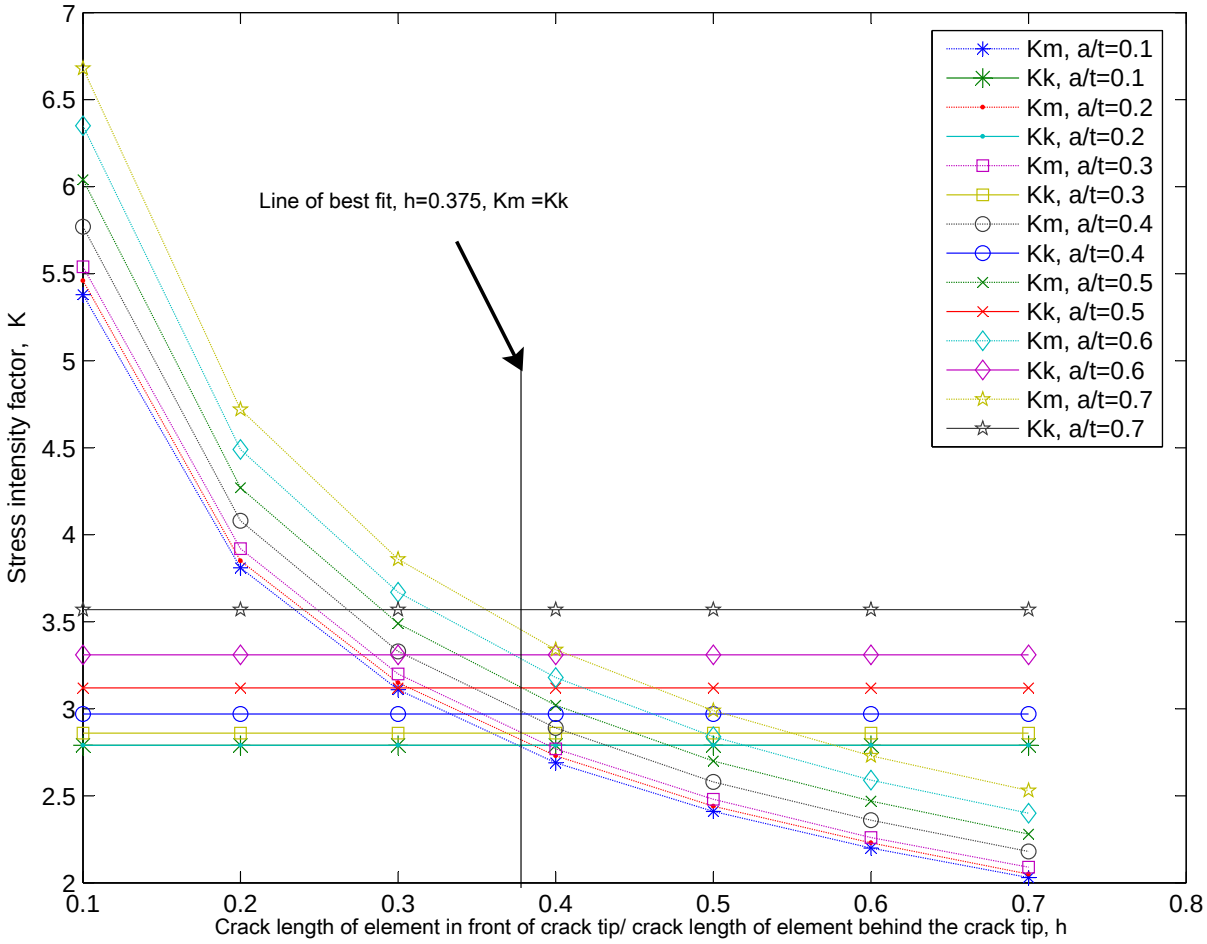

Figure 5.5: Variation of K_m with h for Y=2.0

5.3 Stress intensity factors for cylinders with a single crack

Stress intensity factors for cylinders with a single crack were obtained using the modified virtual crack closure technique and compared with those already in literature [26]. This was done for cylinders with Y=1.5, Y=2.0 and Y=2.5. There was good agreement with the published results for $0.1 \leq a/t \leq 0.7$. Figures 5.6 to 5.8 shows the comparison of the results obtained whereas Table A.5 to A.7 in the appendix shows the actual values obtained. K_m refers to the results obtained using the modified virtual crack closure technique whereas K_k refers to those obtained from literature [26]. The stress intensity factor was found to increase as the length of the cracks were increased. This was because, as the crack length increased, the area of the crack face under pressure increased. Since force is a product of both area and pressure, the increased area resulted in increased circumferential force at the crack tip. The stress intensity factor was found to decrease with increasing diameter ratio of the cylinder. This was because, cylinders with a large diameter ratio are stronger than those with a small diameter ratio.

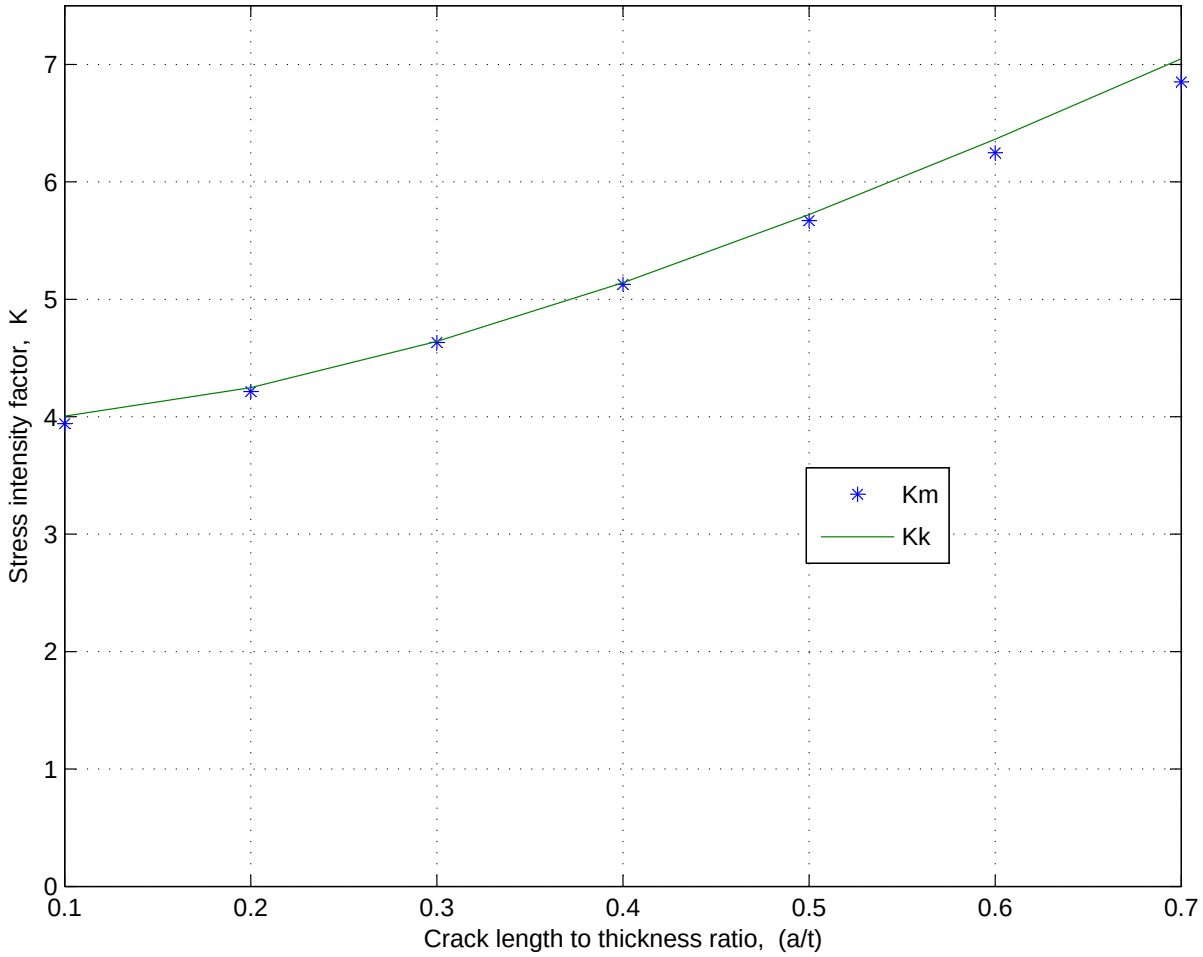

Figure 5.6: Comparison of K_m with K_k for Y=1.5

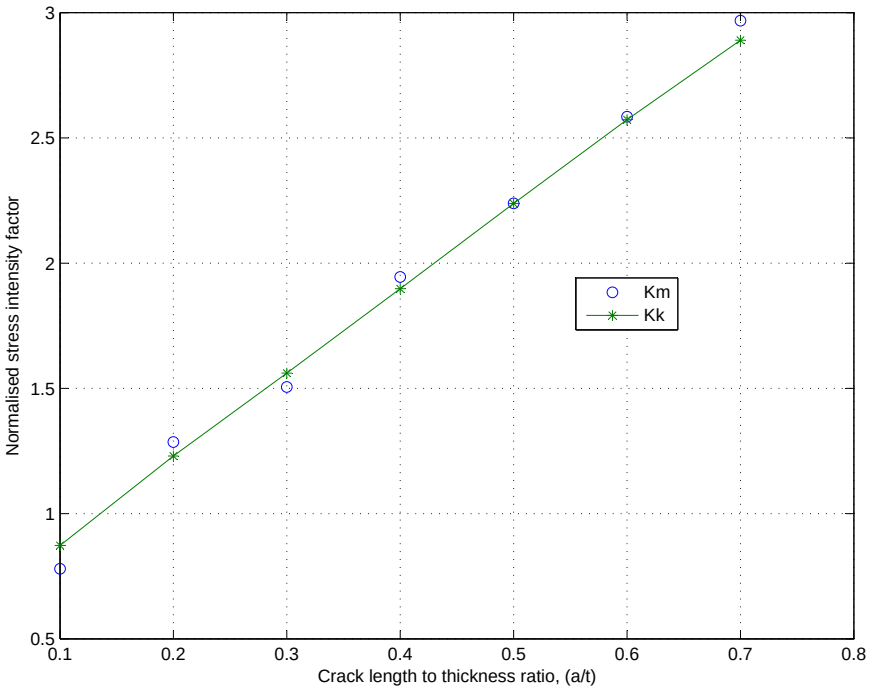

Figure 5.7: Comparison of K_m with K_k for Y=2.0

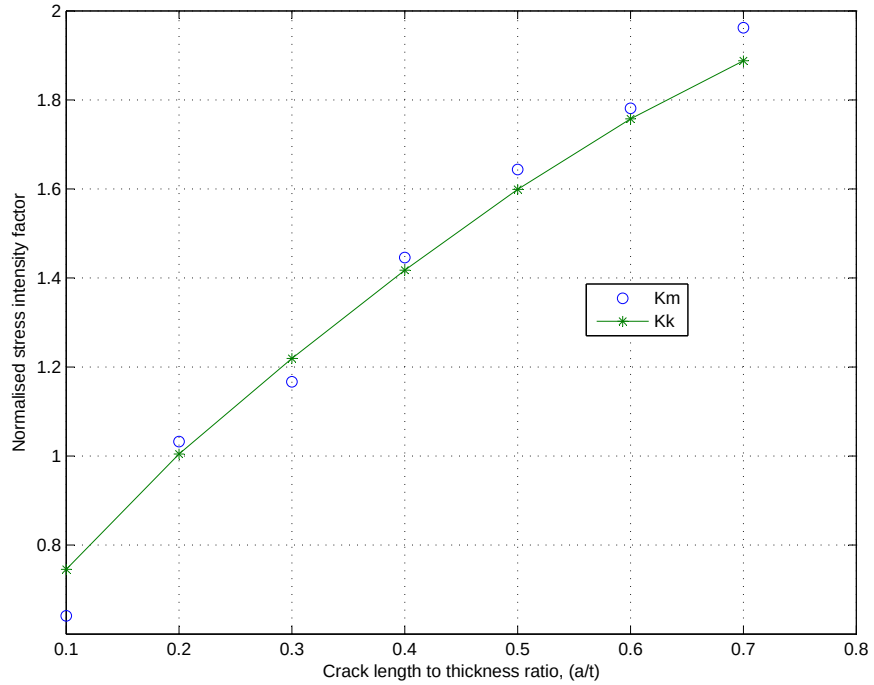

Figure 5.8: Comparison of K_m with K_k for Y=2.5

5.4 Stress intensity factors for cylinders with multiple cracks

The stress intensity factors were calculated for $1 \leq n \leq 100$, $1.5 \leq Y \leq 2.5$ and $0.1 \leq a/t \leq 0.7$. The values obtained were compared with those in literature [26]. The maximum value of K was found to occur when n=2. As the number of cracks increase, the value of K decreases. K also increases with a/t but decreases as Y increases. Figures 5.9 to 5.10 show the variation of K with n for various a/t ratios when Y is constant. For the sake of clarity, graphs of the variation of K with n at various a/t and Y ratios are also presented in Figures 5.11 to 5.16. The actual values of K in Figure 5.9 to Figure 5.16 are listed in Table A.8 to Table A.10 in the appendix.

From Figure 5.9, it was evident that for any a/t ratio, the highest value of K_m occurred when n=2. This was in agreement with what had been reported earlier in literature that the two diametrically opposed cracks 'assist' each other in weakening the cylinder [23]. It was also evident from the figure that K_m decreased as n increased from 2. This was attributed to the concept of load relief whereby the crack opening forces due to the applied pressure were shared by the increasing number of cracks. For $n<10$, the stress intensity factor was found to increase with a/t and this was mainly due to the fact that, as a/t increased, the remaining cylinder thickness in front of the crack tip was decreasing and the gap between the two pressurized crack faces at the crack tip was reducing. The cracks also being far apart meant there was no interaction with the forces acting on neighboring cracks.

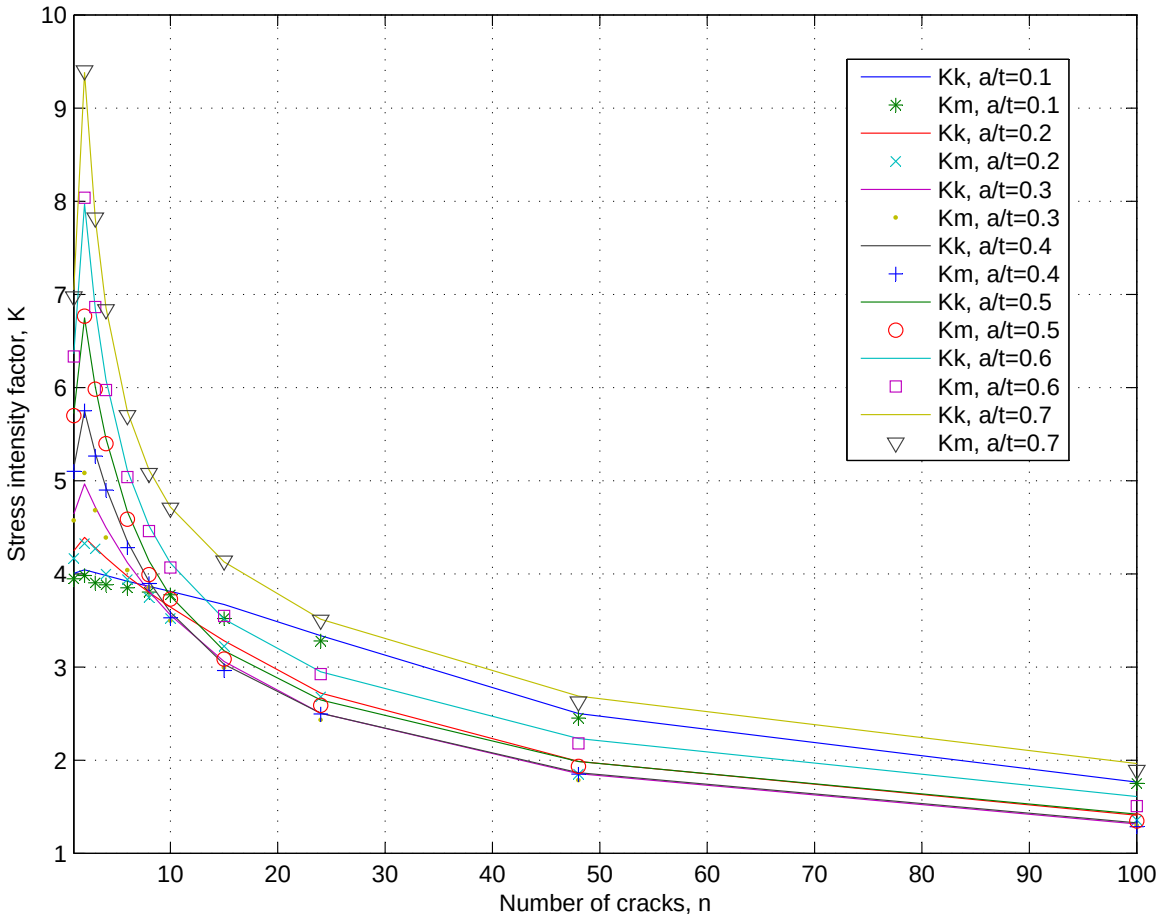

Figure 5.9: K values for a thick-walled cylinder with multiple cracks and Y=1.5

For n>10, the value of K_m was found to generally decrease with a decreasing value of a/t except for a/t=0.1 where the values of K_m are nearly equal to the values of K_m when a/t=0.7. The high values of K_m when a/t=0.1 were attributed to the high hoop stress near the inner surface of the cylinder. The values of K_m in Figure 5.9 were in good agreement with those obtained from literature.

The results in Figure 10(a) and Figure 10(b) displayed a similar trend with those in Figure 5.9. It was however noted that the values of the stress intensity factors in the three figures decreased as Y increased. This was because the strength of the cylinders increases with an increasing value of Y.

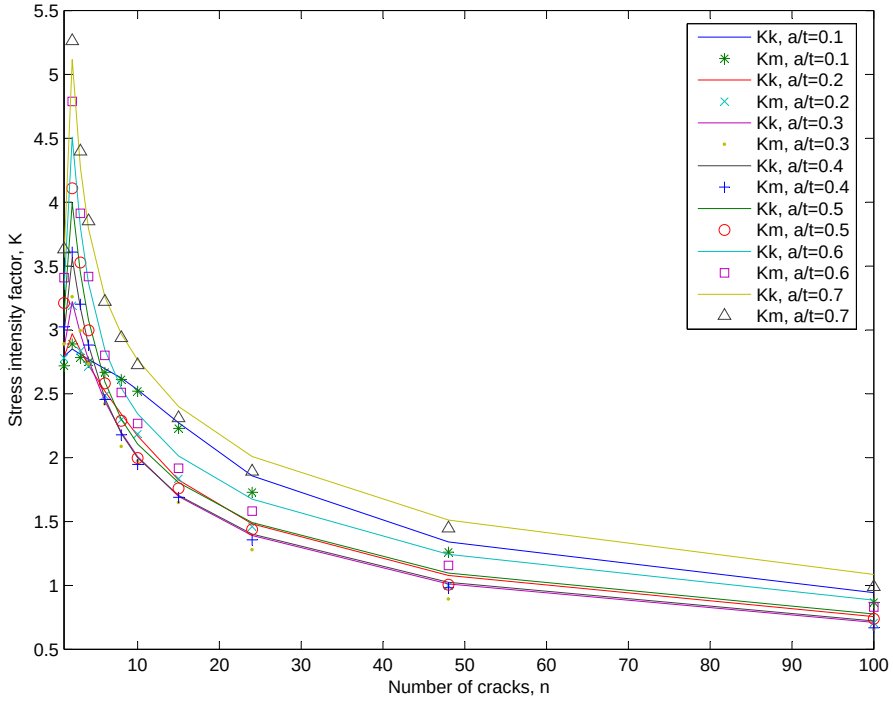

(a) K values Y=2.0

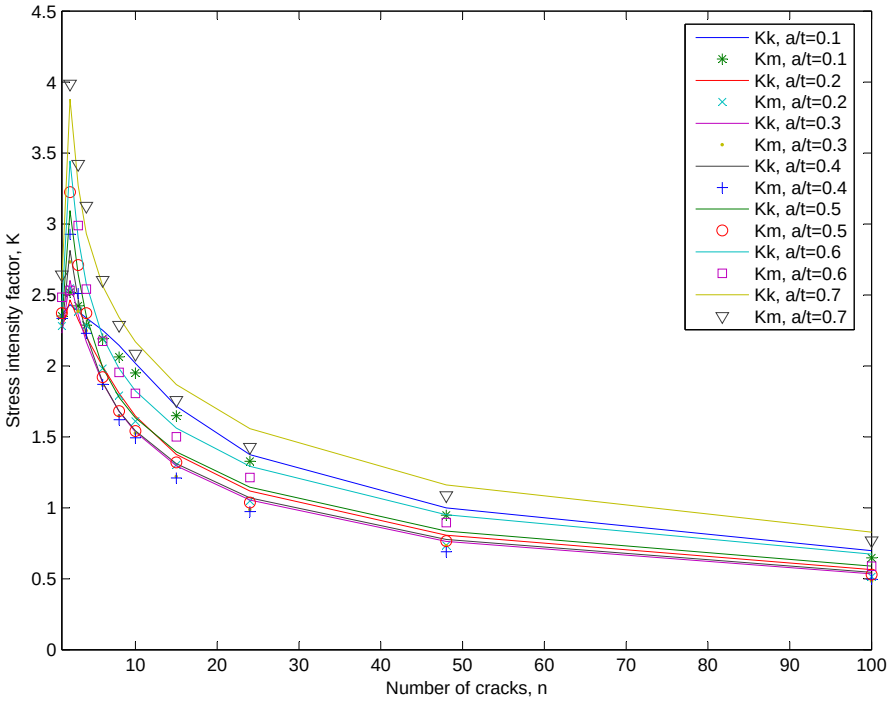

(b) K values Y=2.5

Figure 5.10: K values for cylinders with Y=2.0 and Y=2.5

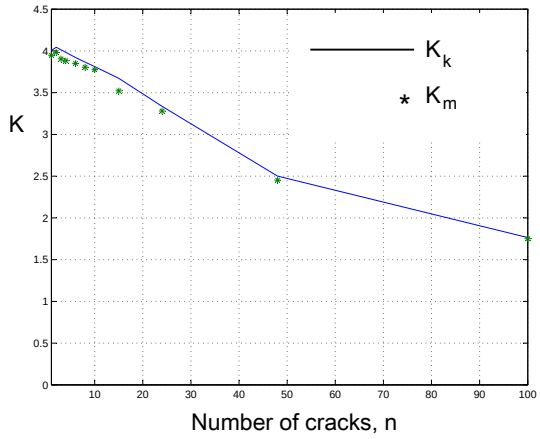

(a) Y=1.5, a/t=0.1

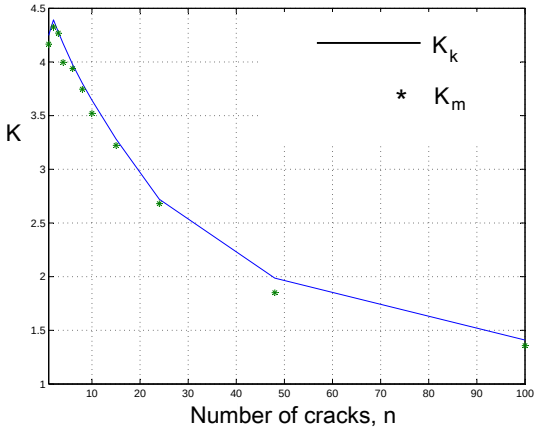

(b) Y=1.5, a/t=0.2

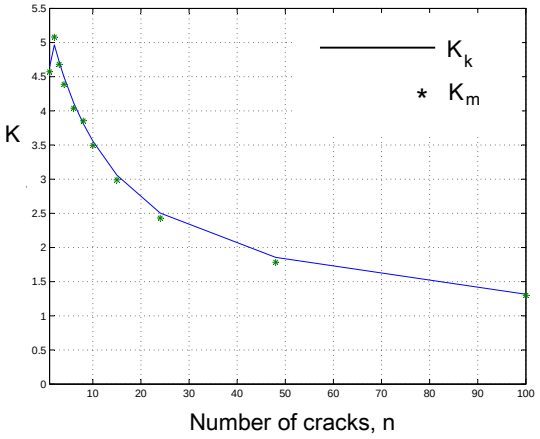

(c) Y=1.5, a/t=0.3

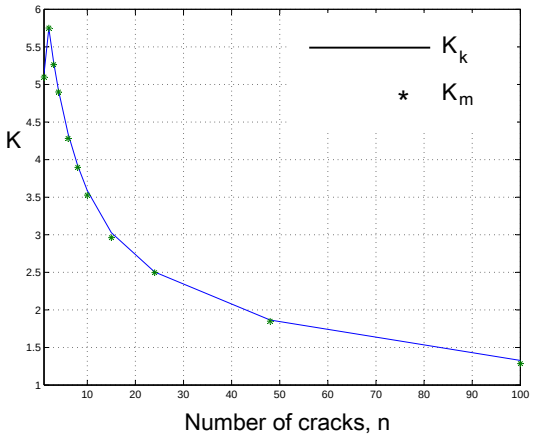

(d) Y=1.5, a/t=0.4

Figure 5.11: K values for Y=1.5, a/t=0.1 to Y=1.5, a/t=0.4

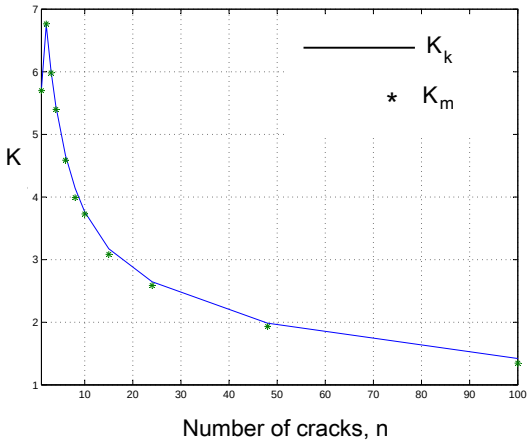

(a) Y=1.5, a/t=0.5

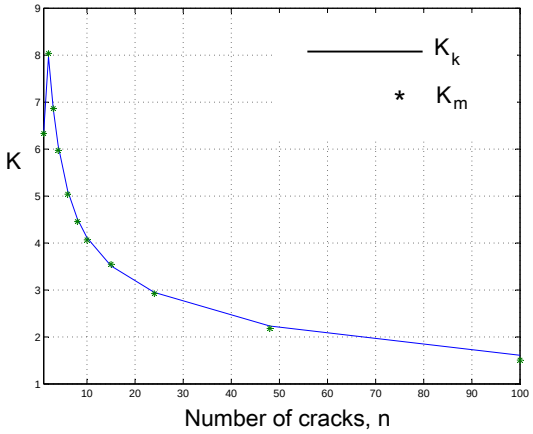

(b) Y=1.5, a/t=0.6

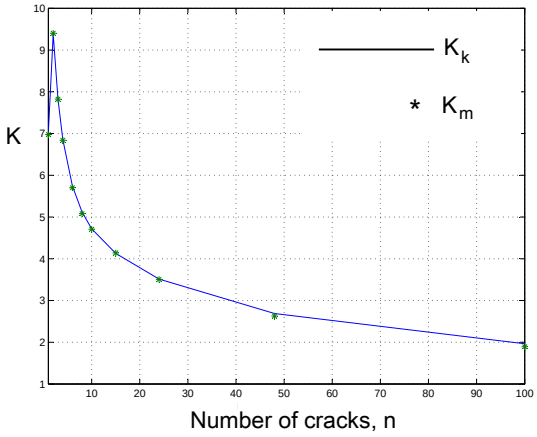

(c) Y=1.5, a/t=0.7

Figure 5.12: K values for Y=1.5, a/t=0.5 to Y=1.5, a/t=0.7

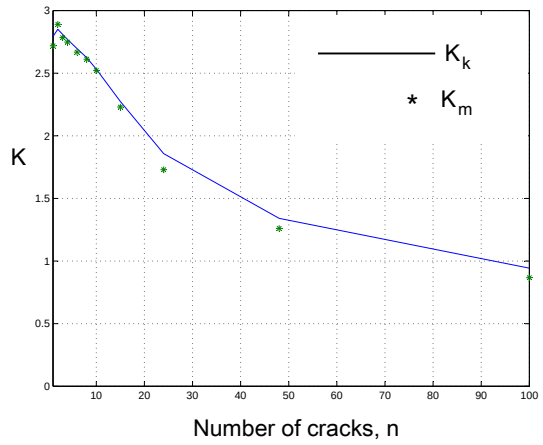

(a) Y=2.0, a/t=0.1

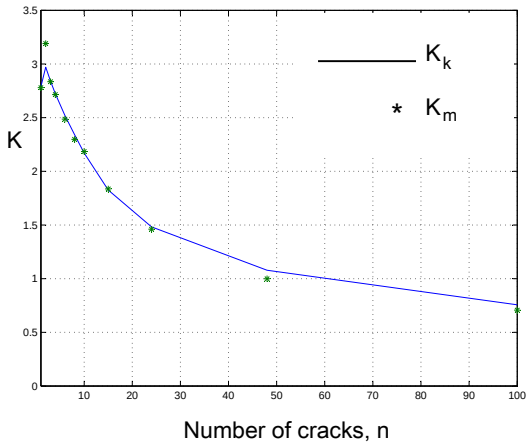

(b) Y=2.0, a/t=0.2

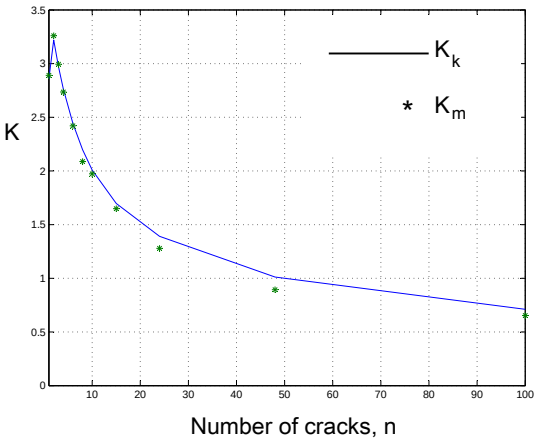

(c) Y=2.0, a/t=0.3

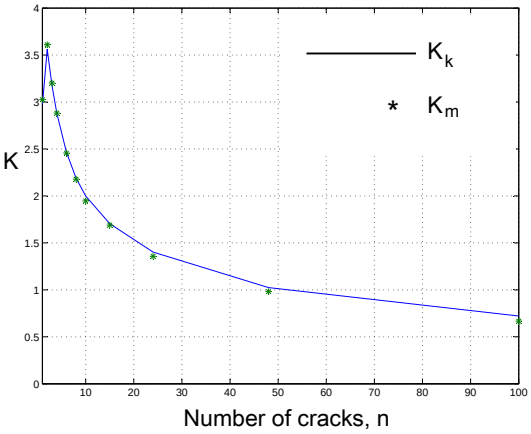

(d) Y=2.0, a/t=0.4

Figure 5.13: K values for Y=2.0, a/t=0.1 to Y=2.0, a/t=0.4

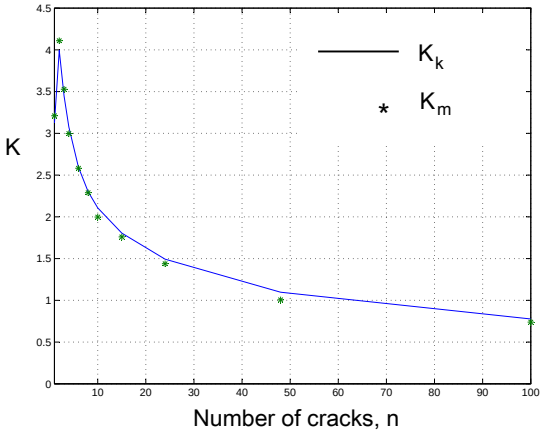

(a) Y=2.0, a/t=0.5

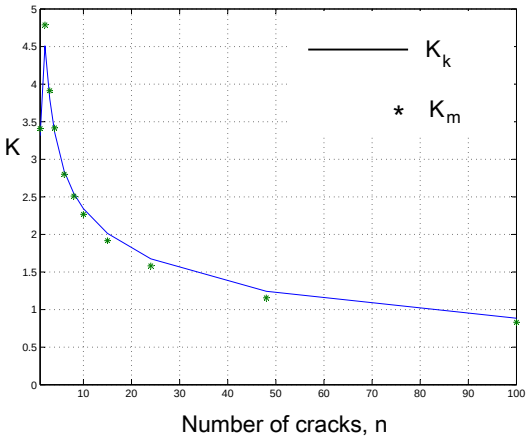

(b) Y=2.0, a/t=0.6

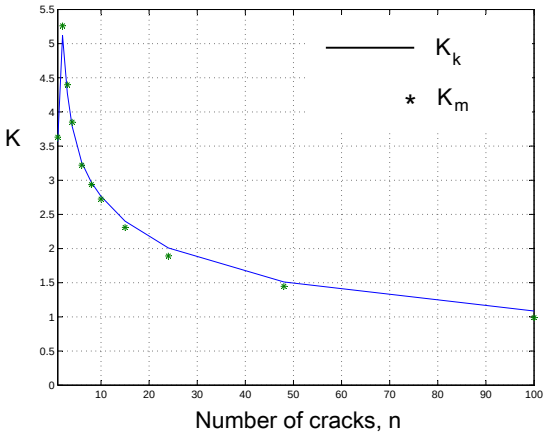

(c) Y=2.0, a/t=0.7

Figure 5.14: K values for Y=2.0, a/t=0.5 to Y=2.0, a/t=0.7

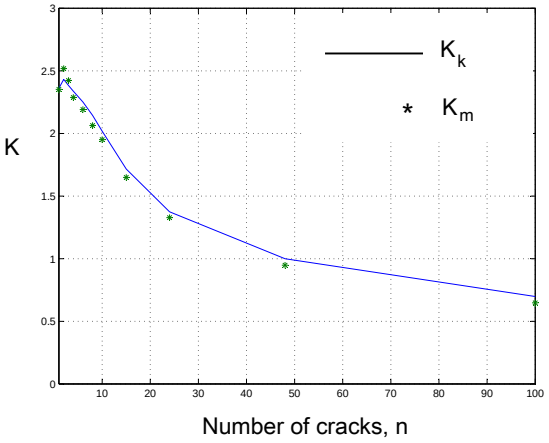

(a) Y=2.5, a/t=0.1

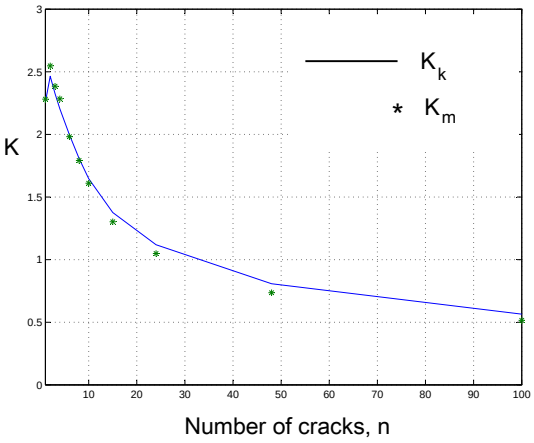

(b) Y=2.5, a/t=0.2

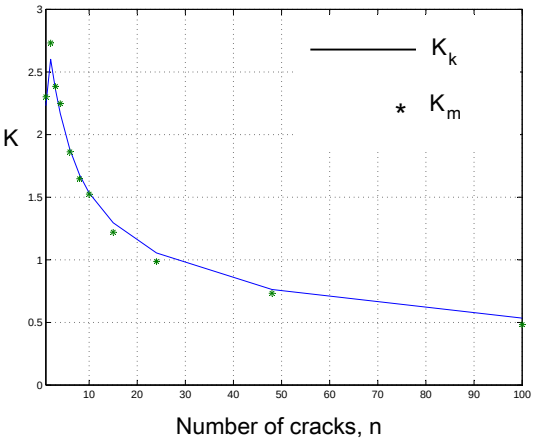

(c) Y=2.5, a/t=0.3

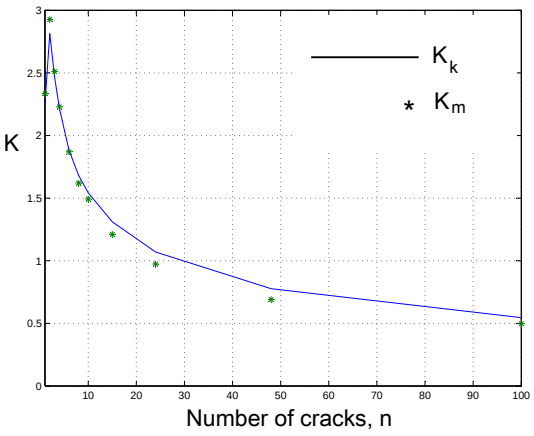

(d) Y=2.5, a/t=0.4

Figure 5.15: K values for Y=2.5, a/t=0.1 to Y=2.5, a/t=0.4

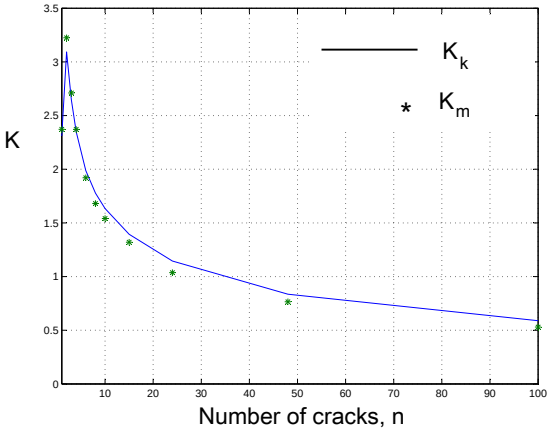

(a) Y=2.5, a/t=0.5

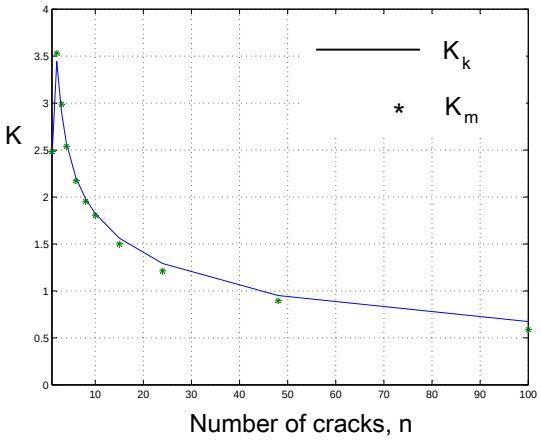

(b) Y=2.5, a/t=0.6

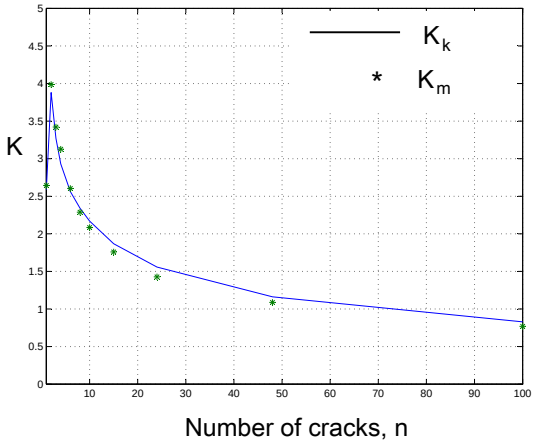

(c) Y=2.5, a/t=0.7

Figure 5.16: K values for Y=2.5, a/t=0.5 to Y=2.5, a/t=0.7

CHAPTER 6

CONCLUSIONS AND RECOMMENDATIONS

6.1 CONCLUSIONS

The aim of this work was to use the modified virtual crack closure technique to obtain the stress intensity factors in multiply cracked thick walled cylinders. The Ansys10 Finite Element Analysis software was used to obtain the nodal forces at the crack tip and the nodal displacements near the crack tip. These parameters enabled the determination of K values for cylinders with different diameter ratios, crack length to thickness ratio and number of cracks. The solid-Tet-10node-187 elements were used in meshing the models and this was due to their regular arrangement around the crack tip that enabled the nodal displacements to be obtained at a constant distance from the crack tip. The models utilized were validated by comparing the finite element hoop, radial and axial stresses with their corresponding values which were obtained using the Lame's equations. These values were found to be nearly equal along the crack face but very different at the crack tip due to stress concentration in the vicinity of the crack tip. Away from the crack tip, the difference between these stresses was less than 3% in all the cases considered.

It was also observed that the modified virtual crack closure technique could not be applied in the analysis of thick walled cylinders in the same way it had been applied in the analysis of flat plates. Thus the cracks investigated were assumed to extend by 37.5% of the length of the finite element behind the crack tip. In this way the K

values obtained for cylinders with either single or multiple cracks had an error of less than 5% in most cases. In conclusion therefore, the K values obtained for thick walled cylinders were in good agreement with the published results.

6.2 RECOMMENDATIONS FOR FURTHER WORK

- In various engineering applications, it is common to find cylinders in which one or more cracks are longer than the other cracks. This could be caused for example by the presence of flaws within the cylinder thickness. Such cases need to be investigated using the modified virtual crack closure technique (MVCCT) since it has proved to be a reliable method from the results presented in this work.

- It is also common to find cylinders which are either fully or partially autofrettaged in a number of engineering applications. These cases should also be investigated using this method and the results validated using the published results.

- The results obtained in this research were for cases where the internal pressure did not cause yielding at any point in the cylinder. It would therefore be worthwhile to investigate cases where yielding occur in cracked cylinders since these cases have been found to occur in some engineering applications.

- Stress intensity factors in cylinders subjected to external pressure only and those subjected to both internal pressure and external pressure should also be determine since these cases were not considered in this analysis.

- Another case that is worth considering is the effects of thermal gradients which

are normally present in cylinders that are used for handling hot pressurized fluids.

- Circumferential cracks have also been known to occur in thick walled cylinders. Stress intensity factors should also be determined using this method for cylinders with such cracks.

REFERENCES

[1] J.H. Underwood and D.P. Kendall, "Fracture analysis of thick-wall cylinder pressure vessels," *Theoretical and Applied Fracture Mechanics*, vol. 2, pp. 47–58, 1984.

[2] M. Habtemariam, "Fracture analysis of pressure vessel under dynamic loading and thermal effect," Master's thesis, Addis Ababa University, 2009.

[3] ASME, *ASME Boiler and Pressure Vessel Code Viii Division 1.* ASME, 2007.

[4] PEP (Professional Engineering Publishers), *The Pressure Equipment Directive (Imeche Event Publications).* Wiley, 2002.

[5] Yasuhide Asada, "Japanese codes and standards system for boilers and pressure vessels an overview," *American Society of Mechanical Engineers*, vol. 3, pp. 1–6, 2001.

[6] Canadian standards association, *Boiler, pressure vessel, and pressure piping code.* CSA standards, 2009.

[7] Committee ME/1,, *Unfired pressure vessels Advanced design and construction (Supplement to AS 12101989).* Standards Association of Australia, 1990.

[8] Germanischer Lloyd, *Rules and Guidelines.* Germanischer Lloyd, 2009.

[9] Det Norske Veritas, *Oil and Gas Processing systems-Offshore Standard DNV-OS-E201,.* Det Norske Veritas, 2008.

[10] Stoomwezen, *Rules for pressure vessels.* Sdu Publishers, 1997.

[11] Chevron corporation, "Welding fundamentals," *Welding manual*, vol. 1, pp. 46–59, 1998.

[12] Kare Hellan, *Introduction to fracture mechanics*. McGraw-Hill book company, 1984.

[13] H. Adldoost, A. Zabihollah, S. J. Fattahi, "Measurement of wall loss in pressure vessels using fbg sensors," *http://journaltool.asme.org/PDF/PVT/11-1042/DRAFT-PVT-11-1042-0.pdf*, vol. 1, pp. 1–8, 2011.

[14] R. Chandwani, M. Wiehahn and C. Timbrell, "3d fracture mechanics in ansys," in *UK ANSYS Conference*, 2004.

[15] "www.ecolo.org/archives/archives-nuc-en/."

[16] F. I. Baratta, "Stress intensity factors for internal multiple cracks in thick-walled cylinders stressed by internal pressure using load relief factors," *Engineering Fracture Mechanics*, vol. 10, pp. 691–697, 1978.

[17] R. Arone and M. Perl, "Stress intensity factors for a pressurized thick-walled cylinder with radial cracks of unequal length," *International Journal of Fracture*, vol. 34, pp. 75–78, 1987.

[18] M. Perl, "Stress intensity factor approximate formulae for uniform crack arrays in pressurized or autofrettaged cylinders," *Engineering Fracture Mechanics*, vol. 5, pp. 725–732, 1992.

[19] Y. H. Zhang, Z.Z. Huang, L. Y. Chen and B. Z. Pan, "A study of the stress intensity factors for single or multiple cracks in thick-walled cylinders," *Nuclear Engineering and Design*, vol. 129, pp. 277–285, 1991.

[20] P. M. G. P. Moreira, "A contribution to the study of fatigue of riveted lap joints," Master's thesis, FEUP- Faculdade de Engendaharia da Universidade do Porto. Portugal, 2004.

[21] B. D. Goldthorpe, "Case studies in fracture mechanics," tech. rep., Army Materials and Mechanics Research Center, Watertown, 1977.

[22] G. Clark and M. E. Morton, "multiple cracking in thick-walled pressure vessels," *International Journal of Fracture*, vol. 15, pp. 17–20, 1979.

[23] R. W. E. Shannon, "Stress intensity factors for thick-walled cylinders," *International Journal of Pressure Vessels and Piping*, vol. 2, pp. 19–24, 1974.

[24] C. P. Andrasic and A. P. Parker, "Dimensionless stress intensity factors for cracked thick cylinders under polynomial crack face loadings," *Engineering Fracture Mechanics*, vol. 19, pp. 187–193, 1984.

[25] K. J. Kirkhope, R. Bell and J. Kirkhope, "Stress intensity factor equations for single and multiple cracked pressurized thick-walled cylinders," *International Journal of Pressure Vessels and Piping*, vol. 41, pp. 103–111, 1990.

[26] H. M. Shu, J. Petit and G. Bezine, "Stress intensity factors for radial symmetrical cracks in thick-walled cylinders.," *Engineering Fracture Mechanics*, vol. 49, pp. 611–623, 1994.

[27] K. Ramesh, S. Shukla, P. M. Dixit and N. Karuppaiah, "Numerical evaluation of stress intensity factor for radial cracks in thick annular ring using cyclic symmetry," *Engineering Fracture Mechanics*, vol. 56, pp. 141–153, 1997.

[28] Y. Z. Chen and H. Y. Liu, "Multiple cracks in pressurized hollow cylinder," *Applied Fracture Mechanics*, vol. 10, pp. 213–218, 1988.

[29] M. Perl and R. Arone, "Stress intensity factors for large arrays of radial cracks in thick-walled steel cylinders," *Engineering Fracture Mechanics*, vol. 25, pp. 341–348, 1986.

[30] C. L. Tan and M. L. Shim, "Stress intensity factor influence coefficients for internal surface cracks in thick-walled cylinders," *International Journal of Pressure Vessels and Piping*, vol. 24, pp. 49–72, 1986.

[31] C.J. Wu, M.C. Hsieh, C.C. Chiu, M.C. Yew and K.N. Chiang, "Interfacial delamination investigation between copper bumps in 3 dimensional chip stacking package by using the modified virtual crack closure technique," *Microelectronic Engineering*, vol. 88, pp. 739–744, 2011.

[32] A. Kumar, S. Gopalakrishnan and A. Chakraborty, "Modified virtual crack closure technique using spectral element method," *International Journal of Computational Methods*, vol. 4, pp. 109–139, 2007.

[33] D. Broek, *Elementary Engineering Fracture Mechanics*. Martinus Nijhoff Publishers, 1982.

[34] H. Sun, S. Rajendran and D. Q. Song, "Finite element analysis on delamination fracture toughness of composite specimen," *Proceedings of 2nd Asian ANSYS User Conference*, vol. 2, pp. 1–8, 1998.

[35] S. M. O. Tavares, P. M. G. P. Moreira, S. D. Pastrama and P. M. S. T. Castro, "Stress intensity factors by numerical evaluation in cracked structures," tech. rep., Department of mechanical engineering Faculdade de Engendaharia da Universidade do Porto, Portugal. Department of strength of materials, University "Politehnica" of Bucharest Romania, 2004.

[36] J. Schijve, *Fatigue of Structures and Materials*. Springer, 2001.

[37] D. J. Cartwright and D. P. Rooke, "Approximate stress intensity factors compounded from known solutions," *Engineering fracture mechanics*, vol. 6(3), pp. 563–571, 1974.

[38] S. M. O. Tavares, P. M. G. P. Moreira, S. D. Pastrama and P. M. S. T. Castro, "Introduction to the method and the case of cracked stiffened plates," in *Compounded stress intensity factors*, 2006.

[39] P. C. Paris and G. C. Sih, "Stress analysis of cracks. in fracture toughness testing and its applications," *ASTM American Society for Testing and Materials*, vol. ASTM STP 381, pp. 30–83, 1965.

[40] S. Raju and J. C. Newman Jr, "Three dimensional finite-element analysis of finite-thickness fracture specimens," tech. rep., Langley Research Center NASA TN D-8414, 1977.

[41] S. Bist and R. Kannusamy, "Predicting 3-d fatigue cracks without a crystal ball," *ANSYS advantage*, vol. 3, pp. 31–32, 2009.

[42] J. R. Rice, "Mathematical analysis in the mechanics of fracture," *In Fracture - An advanced treatise*, vol. II, pp. 191–308, 1968.

[43] R. Krueger and D. Goetze, "Influence of finite element software on energy release rates computed using the virtual crack closure technique," tech. rep., National Institute of Aerospace (NIA) and National Aeronautics and Space Administration (NASA), 2006.

[44] R. Krueger, "The virtual crack closure technique, history, approach and applications,," tech. rep., NASA Langley Research Center, Hampton, 2002.

[45] E. F. Rybicki and M. F. Kanninen, "Finite-element calculation of stress intensity factors by a modified crack closure integrals," *Engineering Fracture Mechanics*, vol. 9(4), pp. 931–938, 1977.

Appendix A

Actual values of normalized stresses and stress intensity factors

Table A.1: Un-cracked cylinder stresses versus finite element stresses along the crack for Figure 4.9

e/f	$\frac{\sigma_r}{\sigma_y}$ for an un-cracked cylinder X 10^{-2}	Finite element's $\frac{\sigma_r}{\sigma_y}$ for a cracked cylinder X 10^{-2}	$\frac{\sigma_\theta}{\sigma_y}$ for an un-cracked cylinder X 10^{-2}	Finite element's $\frac{\sigma_\theta}{\sigma_y}$ for a cracked cylinder X 10^{-2}	$\frac{\sigma_l}{\sigma_y}$ for an un-cracked cylinder X 10^{-2}	Finite element's $\frac{\sigma_l}{\sigma_y}$ for a cracked cylinder X 10^{-2}
0	-0.72	-0.72	1.88	-0.89	0.58	0.69
0.22	-0.72	-0.72	1.88	-0.76	0.58	0.76
0.43	-0.72	-0.78	1.88	-0.76	0.58	0.72
0.44	-0.66	-0.81	1.82	-0.73	0.58	0.69
0.46	-0.52	-1.32	1.68	-0.72	0.58	0.54
0.48	-0.39	-1.78	1.54	-0.74	0.58	-0.13
0.49	-0.29	-1.56	1.45	-1.14	0.58	-1.58
0.50	-0.26	-26.67	1.41	36.31	0.58	18.10
0.51	-0.29	-1.56	1.45	-1.14	0.58	-1.58
0.52	-0.39	-1.78	1.54	-0.74	0.58	-0.13
0.54	-0.52	-1.32	1.68	-0.72	0.58	0.54
0.56	-0.66	-0.81	1.82	-0.73	0.58	0.69
0.57	-0.72	-0.78	1.88	-0.76	0.58	0.72
0.78	-0.72	-0.72	1.88	-0.76	0.58	0.76
1.00	-0.72	-0.72	1.88	-0.89	0.58	0.69

Table A.2: Theoretical versus finite element stresses for Figure 5.1

x/t X 10^{-2}	Finite element $\frac{\sigma_r}{\sigma_y}$ X 10^{-2}	Theoretical $\frac{\sigma_r}{\sigma_y}$ for an un-cracked cylinder X 10^{-2}	Finite element $\frac{\sigma_\theta}{\sigma_y}$ X 10^{-2}	Theoretical $\frac{\sigma_\theta}{\sigma_y}$ for an un-cracked cylinder X 10^{-2}	Finite element $\frac{\sigma_l}{\sigma_y}$ X 10^{-2}	Theoretical $\frac{\sigma_l}{\sigma_y}$ for an un-cracked cylinder X 10^{-2}
0.00	-0.72	-0.72	-0.71	1.88	0.62	0.58
0.59	-0.82	-0.65	-0.72	1.81	0.61	0.58
1.40	-1.12	-0.56	-0.73	1.72	0.58	0.58
2.50	-1.51	-0.45	-0.75	1.61	0.57	0.58
36.00	-1.90	-0.36	-0.85	1.52	0.27	0.58
44.00	-1.77	-0.30	-0.93	1.46	-1.13	0.58
50.00	34.11	-0.26	47.60	1.41	22.54	0.58
56.00	7.35	-0.22	7.48	1.38	1.22	0.58
64.00	3.09	-0.17	4.10	1.33	0.44	0.58
75.00	1.33	-0.11	2.04	1.27	0.56	0.58
86.00	0.48	-0.06	0.40	1.22	0.58	0.58
94.00	0.12	-0.02	0.92	1.18	0.57	0.58
100.00	0.00	0.00	-2.15	1.16	0.55	0.58

Table A.3: Variation of h with K_m when Y=1.5

a/t / h	0.1		0.2		0.3		0.4		0.5		0.6		0.7	
	K_m	K_k	K_m	K_k	K_m	K_k	K_m	K_k	K_m	K_k	K_m	K_k	K_m	K_k
0.1	7.62	4.01	8.15	4.25	8.97	4.64	9.93	5.14	10.98	5.72	12.10	6.36	13.27	7.05
0.2	5.40	4.01	5.76	4.25	6.34	4.64	7.02	5.14	7.76	5.72	8.56	6.63	9.38	7.05
0.3	4.41	4.01	4.71	4.25	5.18	4.64	5.74	5.14	6.34	5.72	6.99	6.36	7.66	7.05
0.4	3.81	4.01	4.08	4.25	4.48	4.64	4.97	5.14	5.49	5.72	6.05	6.36	6.63	7.05
0.5	3.41	4.01	3.65	4.25	4.01	4.64	4.44	5.14	4.91	5.72	5.41	6.36	5.93	7.05
0.6	3.11	4.01	3.33	4.25	3.66	4.64	4.06	5.14	4.48	5.72	4.94	6.36	5.42	7.05
0.7	2.88	4.01	3.08	4.25	3.39	4.64	3.75	5.14	4.15	5.72	4.57	6.36	5.01	7.05

Table A.4: Variation of h with K_m when Y=2.0

a/t / h	0.1		0.2		0.3		0.4		0.5		0.6		0.7	
	K_m	K_k	K_m	K_k	K_m	K_k	K_m	K_k	K_m	K_k	K_m	K_k	K_m	K_k
0.1	5.38	2.79	5.46	2.79	5.54	2.86	5.77	2.97	6.04	3.12	6.35	3.31	6.68	3.57
0.2	3.81	2.79	3.85	2.79	3.92	2.86	4.08	2.97	4.27	3.12	4.49	3.31	4.72	3.57
0.3	3.11	2.79	3.15	2.79	3.20	2.86	3.33	2.97	3.49	3.12	3.67	3.31	3.86	3.57
0.4	2.69	2.79	2.73	2.79	2.77	2.86	2.89	2.97	3.02	3.12	3.18	3.31	3.34	3.57
0.5	2.41	2.79	2.44	2.79	2.48	2.86	2.58	2.97	2.70	3.12	2.84	3.31	2.99	3.57
0.6	2.20	2.79	2.23	2.79	2.26	2.86	2.36	2.97	2.47	3.12	2.59	3.31	2.73	3.57
0.7	2.03	2.79	2.05	2.79	2.09	2.86	2.18	2.97	2.28	3.12	2.40	3.31	2.53	3.57

Table A.5: Dimensionless K values for a cylinder with 1 crack and Y=1.5

a/t	K_m	K_k
0.1	3.94	4.01
0.2	4.21	4.25
0.3	4.63	4.64
0.4	5.13	5.14
0.5	5.67	5.72
0.6	6.25	6.36
0.7	6.85	7.05

Table A.6: Dimensionless K values for a cylinder with 1 crack and Y=2.0

a/t	K_m	K_k
0.1	2.78	2.79
0.2	2.79	2.79
0.3	2.86	2.86
0.4	2.98	2.97
0.5	3.12	3.12
0.6	3.26	3.31
0.7	3.45	3.57

Table A.7: Dimensionless K values for a cylinder with 1 crack and Y=2.5

a/t	K_m	K_k
0.1	2.30	2.36
0.2	2.26	2.26
0.3	2.28	2.23
0.4	2.31	2.25
0.5	2.37	2.31
0.6	2.43	2.41
0.7	2.51	2.59

Table A.8: Dimensionless K values for a multiply cracked cylinder with Y=1.5

a/t \ n	0.1		0.2		0.3		0.4		0.5		0.6		0.7	
	K_m	K_k	K_m	K_k	K_m	K_k	K_m	K_k	K_m	K_k	K_m	K_k	K_m	K_k
1	4.01	3.95	4.25	4.17	4.64	4.57	5.14	5.10	5.72	5.70	6.36	6.33	7.05	6.98
2	4.04	3.98	4.39	4.33	4.97	5.08	5.75	5.75	6.75	6.77	7.97	8.04	9.38	9.40
3	4.01	3.90	4.28	4.27	4.72	4.68	5.30	5.26	6.01	5.98	6.85	6.86	7.82	7.82
4	3.98	3.88	4.17	4.00	4.50	4.39	4.93	4.90	5.45	5.40	6.08	5.97	6.86	6.84
6	3.92	3.85	3.98	3.94	4.12	4.04	4.34	4.28	4.67	4.59	5.11	5.04	5.74	5.70
8	3.87	3.80	3.80	3.75	3.81	3.85	3.92	3.90	4.14	3.99	4.52	4.46	5.12	5.08
10	3.81	3.78	3.64	3.52	3.56	3.50	3.59	3.53	3.76	3.73	4.11	4.07	4.72	4.71
15	3.67	3.52	3.28	3.22	3.06	2.99	3.03	2.96	3.17	3.08	3.51	3.55	4.13	4.14
24	3.34	3.28	2.72	2.68	2.50	2.43	2.50	2.50	2.65	2.59	2.95	2.92	3.51	3.50
48	2.50	2.45	1.99	1.85	1.86	1.78	1.87	1.85	1.98	1.93	2.23	2.18	2.69	2.63
100	1.76	1.75	1.41	1.36	1.32	1.30	1.33	1.29	1.42	1.35	1.61	1.51	1.96	1.89

Table A.9: Dimensionless K values for a multiply cracked cylinder with Y=2.0

a/t \ n	0.1		0.2		0.3		0.4		0.5		0.6		0.7	
	K_m	K_k	K_m	K_k	K_m	K_k	K_m	K_k	K_m	K_k	K_m	K_k	K_m	K_k
1	2.79	2.72	2.79	2.78	2.86	2.89	2.97	3.02	3.12	3.21	3.31	3.41	3.57	3.63
2	2.85	2.89	2.97	3.19	3.22	3.26	3.56	3.61	3.99	4.11	4.51	4.79	5.12	5.26
3	2.81	2.78	2.84	2.84	2.97	2.99	3.17	3.20	3.45	3.53	3.81	3.91	4.27	4.40
4	2.77	2.75	2.72	2.72	2.76	2.74	2.88	2.88	3.08	3.00	3.36	3.42	3.80	3.85
6	2.70	2.67	2.52	2.49	2.44	2.42	2.47	2.46	2.59	2.58	2.84	2.80	3.26	3.22
8	2.62	2.61	2.34	2.30	2.20	2.09	2.19	2.18	2.30	2.29	2.54	2.51	2.97	2.94
10	2.53	2.52	2.17	2.18	2.01	1.97	2.00	1.95	2.11	2.00	2.34	2.27	2.76	2.72
15	2.27	2.23	1.83	1.84	1. 70	1.65	1.70	1.69	1.81	1.76	2.01	1.92	2.40	2.31
24	1.86	1.73	1.48	1.46	1.39	1.28	1.40	1.36	1.49	1.44	1.68	1.58	2.01	1.89
48	1.34	1.26	1.08	1.00	1.01	0.89	1.02	0.98	1.10	1.01	1.24	1.16	1.51	1.45
100	0.94	0.87	0.76	0.71	0.71	0.65	0.72	0.67	0.78	0.74	0.88	0.83	1.09	0.99

Table A.10: Dimensionless K values for a multiply cracked cylinder with Y=2.5

a/t \ n	0.1		0.2		0.3		0.4		0.5		0.6		0.7	
	K_m	K_k	K_m	K_k	K_m	K_k	K_m	K_k	K_m	K_k	K_m	K_k	K_m	K_k
1	2.36	2.35	2.26	2.28	2.23	2.30	2.25	2.33	2.31	2.37	2.41	2.48	2.59	2.64
2	2.43	2.52	2.46	2.54	2.60	2.73	2.81	2.93	3.09	3.22	3.44	3.53	3.88	3.99
3	2.38	2.42	2.33	2.38	2.36	2.38	2.47	2.51	2.64	2.71	2.90	2.99	3.27	3.42
4	2.34	2.29	2.21	2.28	2.17	2.25	2.22	2.23	2.35	2.37	2.58	2.54	2.93	3.13
6	2.25	2.19	2.00	1.98	1.88	1.86	1.88	1.87	1.99	1.92	2.20	2.17	2.56	2.60
8	2.14	2.06	1.81	1.79	1.68	1.65	1.68	1.62	1.78	1.68	1.98	1.95	2.34	2.29
10	2.02	1.95	1.65	1.61	1.53	1.52	1.54	1.49	1.63	1.54	1.82	1.81	2.17	2.08
15	1.72	1.65	1.38	1.30	1.30	1.22	1.31	1.21	1.39	1.32	1.56	1.50	1.87	1.76
24	1.37	1.33	1.12	1.05	1.05	0.99	1.07	0.97	1.15	1.04	1.29	1.21	1.56	1.43
48	1.00	0.95	0.81	0.74	0.76	0.73	0.78	1.69	0.84	0.77	0.95	0.90	1.16	1.09
100	0.70	0.65	0.57	0.51	0.53	0.48	0.55	0.50	0.59	0.53	0.67	0.59	0.83	0.77